High-frequency properties of a double-cathode tube

HIGH–FREQUENCY PROPERTIES
OF
A DOUBLE–CATHODE TUBE

W. VERSNEL

HIGH-FREQUENCY PROPERTIES

OF

A DOUBLE-CATHODE TUBE

DOOR

WILLEM VERSNEL

GEBOREN TE ROTTERDAM

DIT PROEFSCHRIFT IS GOEDGEKEURD DOOR DE PROMOTOR
PROF. DR. H. GROENDIJK

Aan mijn Ouders

Aan mijn Vrouw

CONTENTS

1. INTRODUCTION

The behaviour of any two-terminal network can be described by its admittance $Y = g + jb$ and a noise current source i in parallel with Y. When such a network is in thermal equilibrium at temperature T, the mean square of i is given by Nyquist's formula

$$\overline{i^2} = 4 \, k \, T \, g \, \Delta f \qquad\qquad (1.1)$$

where k is Boltzmann's constant and Δf is the band width concerned.

A saturated vacuum diode through which a d.c. current I is flowing gives a short-circuit noise current i. This phenomenon is known as shot noise. For frequencies ω at which the transit times of the electrons are much smaller than $1/\omega$, the shot noise is given by

$$\overline{i^2} = 2 \, q \, I \, \Delta f \qquad\qquad (1.2)$$

where $-q$ is the electronic charge.

If the diode is working in its space-charge limited region, there is a potential minimum somewhere in the inter-electrode space. This potential minimum causes part of the electrons to be reflected, so that only electrons with a sufficiently large emission velocity reach the anode. The amount of noise is then smaller, since fluctuations in the electron emission from the cathode cause fluctuations in the depth of the potential minimum that reduce the current fluctuations. This effect can be taken into account by introducing a noise suppression factor Γ^2 into Eq.(1.2):

$$\overline{i^2} = 2 \, q \, I \, \Gamma^2 \, \Delta f \qquad\qquad (1.3)$$

Assuming that the electrons have a Maxwellian velocity distribution when leaving the cathode and that there are no collisions between the electrons, Γ^2 can be calculated[1] for a plane diode.

Let us now consider a plane diode of symmetrical construction, in which two equal cathodes having the same temperature T are at a small distance d opposite each other. Supposing this double-cathode tube is working in the space-charge region, there is again a potential minimum somewhere between the cathodes. The potential distribution in such a diode (Fig. 1.1) has been calculated by Lindsay et al.[2]
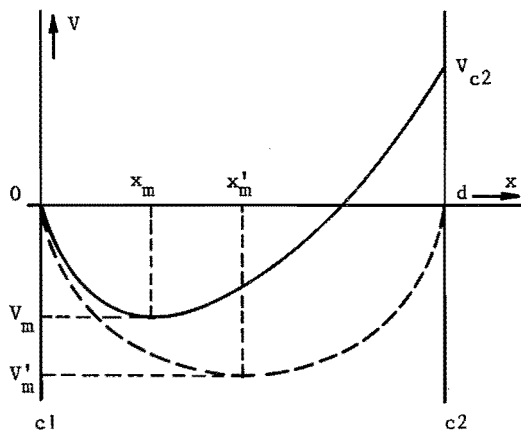
Fig. 1.1. Potential distributions in a plane space-charge limited double-cathode tube if the applied d.c. voltage $V_{c2} \neq 0$ (solid line) and $V_{c2} = 0$ (dotted line). The cathodes c_1 and c_2 have the same temperature T.

If the two cathodes are at the same potential, the d.c. current is zero, but nevertheless electrons are passing from one cathode to the other, and vice versa. Again, fluctuations in the emission currents of the cathodes cause fluctuations in the depth of the potential minimum. However, here the latter fluctuations do not reduce the noise, because a

8

change of its depth has the same influence on the currents of both cath-
odes. Hence, we can calculate the noise by applying Eq.(1.2) for the shot
noise. If I is the d.c. current passing from one cathode to the other,
then the total electron current flowing is 2I, so that

$$\overline{i^2} = 4 \, q \, I \, \Delta f \tag{1.4}$$

On the other hand, this double-cathode tube is a two-terminal network in
thermal equilibrium at cathode temperature T, so that also Eq.(1.1) holds.
Combining this with Eq.(1.4) leads to the following expression for the
conductance[1,3)]

$$g = \frac{qI}{kT} \tag{1.5}$$

If the frequency ω is so high that the transit times of the electrons
are not small compared with $1/\omega$, the noise of a saturated diode is smaller
than that given by Eq.(1.2). Also, for a space-charge limited diode the
noise suppression factor Γ^2 in Eq.(1.3) becomes smaller at high frequen-
cies, because there are now two noise reducing effects, viz. variations
of the depth of the potential minimum and the transit times of the elec-
trons.

For the double-cathode tube at thermal equilibrium Eq.(1.4) is not
found to be true at high frequencies either. Representing the noise by

$$\overline{i^2} = 4 \, q \, I \, \Gamma^2 \, \Delta f \tag{1.6}$$

the noise suppression factor Γ^2 is now caused by transit-time effects
alone.

In this thesis the noise quantity $\overline{i^2}$ and the admittance Y of a double-cathode tube will be calculated at different values of the transit times of the electrons. These values are obtained at a constant frequency of 3 GHz by taking various values of the distance between the two cathodes. Eq.(1.1) provides a check on these calculations, since the temperature T that can be derived from them, and which is called the noise temperature T_n, must be equal to the cathode temperature.

We shall further investigate what happens if a small potential difference ($\le$ 0.5 volt) is put between the cathodes, which are still at the same temperature T. Then thermal equilibrium will no longer exist. Yet, Eq. (1.1) can be used to define a noise temperature T_n but it appears to be lower than the cathode temperature.

In the next chapter we start with a short review of the low-frequency properties of a double-cathode tube. Using a one-dimensional model, it is shown that the average kinetic energy of the electrons in a volume element at any point between the cathodes is $\frac{1}{2}kT$, when the two cathodes have the same temperature and the same potential.

Later chapters are devoted to the high-frequency theory for the admittance and the noise of a double-cathode tube, and to the measurements of these quantities by mounting such a tube in a waveguide, in which only the dominant mode of the electromagnetic field can be propagated. In this tube the distance between the cathodes can be varied.

The calculations further provide a means of investigating the processes going on inside such a tube, if an a.c. voltage is applied between the two cathodes. It is found that space-charge waves start from both cathodes and travel inwards with rapidly decreasing amplitudes.

2. POTENTIAL DISTRIBUTION IN A DOUBLE-CATHODE TUBE. RELATION WITH THERMODYNAMICS

2.1 Introduction

In this chapter a short review is given of the l.f. electric-field strength, the potential distribution, the density of the electrons, etc. These quantities will be used later on. It is assumed that the electrons have a Maxwellian velocity distribution when leaving the cathode and that the tube works in the space-charge region.

It is shown that when the applied d.c. voltage between the cathodes is zero, the average kinetic energy of the electrons in a volume element at any point between the cathodes is $\frac{1}{2}kT$.

Contrary to Lindsay et al.[2], who have analysed a three-dimensional model, we have used a one-dimensional model. Evidently, both models lead to the same results.

2.2 Potential distribution

2.2.1 Phase-space densities

If the two cathodes are kept at different potentials 0 and V_{c2} (Fig. 1.1), then the velocities of the electrons at a point x between the cathodes are given by the following expressions

$$v^2 = v_{c1}^2 + \frac{2q}{m} V \tag{2.1}$$

and

$$v^2 = v_{c2}^2 + \frac{2q}{m} (V - V_{c2}) \tag{2.2}$$

where v is the electron velocity, v_{c1} and v_{c2} are the electron velocities at the two cathodes, and m is the electronic mass.

Let $n(x,v)$ be the phase-space density[4], i.e. $n(x,v)$ dx dv is the

number of electrons per unit area which are situated between x and x+dx

and have velocities between v and v+dv. Now, $n(x,v)$ consists of two parts:

$$n(x,v) = n_1(x,v) + n_2(x,v) \qquad (2.3)$$

where $n_1(x,v)$ and $n_2(x,v)$ are the contributions to $n(x,v)$ of the two

cathodes. The phase-space density $n_1(x,v)$ of electrons leaving cathode

c_1, at $x = 0$, is

$$n_1(0,v_{c1}) = \frac{m}{kTq} J_s \exp\left(-\frac{mv_{c1}^2}{2kT}\right) \qquad (v_{c1} \geq 0) \qquad (2.4)$$

where T is the temperature of the cathodes and J_s is the saturation cur-

rent density. From (2.1) and (2.4) one finds

$$n_1(x,v) = \frac{m}{kTq} J_s \exp\left(\frac{qV}{kT}\right) \exp\left(-\frac{mv^2}{2kT}\right) \qquad (2.5)$$

Similarly, we have for electrons emitted by cathode c_2

$$n_2(x,v) = \frac{m}{kTq} J_s \exp\left\{\frac{q}{kT}(V - V_{c2})\right\} \exp\left(-\frac{mv^2}{2kT}\right) \qquad (2.6)$$

In fact, Eqs.(2.5) and (2.6) are consequences of Liouville's law.

2.2.2 Extreme_velocities_of_electrons

Consider an electron emitted by cathode c_1 which has a velocity

$v_m = 0$, when it is at the potential minimum x_m (Fig. 1.1). Then its ve-

locity at any point x in the inter-electrode space, after reaching the

potential minimum, is the minimum velocity of all electrons leaving c_1:

12

$$v_{min}(x) = \mp \left[\frac{2q}{m} \left\{ V(x) - V_m \right\} \right]^{\frac{1}{2}} \tag{2.7}$$

where the upper sign is valid in region L, which is on the left of the potential minimum x_m, whereas the lower sign refers to region R, which is on the right of x_m. This notation will be used throughout in this thesis.

Similarly, we find for the maximum velocity of the electrons emitted by cathode c_2

$$v_{max}(x) = \mp \left[\frac{2q}{m} \left\{ V(x) - V_m \right\} \right]^{\frac{1}{2}} \tag{2.8}$$

2.2.3 The l.f. electric-field strength E(x)

For plane electrodes Poisson's equation is

$$\frac{d^2 V}{dx^2} = \frac{q}{\varepsilon_o} n(x) \tag{2.9}$$

where $n(x)$ is the volume density of the electrons and ε_o is the dielectric constant of free space. For $n(x)$ the following expression is valid

$$n(x) = \int n(x,v) \, dv$$

where one has to integrate over all possible velocities. It is easy to obtain (Cf.[4])

$$n(x) = \frac{1}{q} \left(\frac{\pi m}{2kT} \right)^{\frac{1}{2}} J_s \exp(\eta) \left[\exp(-\eta_{c1}) \left\{ 1 \pm \text{erf}(\eta^{\frac{1}{2}}) \right\} + \right.$$
$$\left. + \exp(-\eta_{c2}) \left\{ 1 \mp \text{erf}(\eta^{\frac{1}{2}}) \right\} \right] \tag{2.10}$$

with $\eta = (V - V_m)q/kT$, $\eta_{c1} = -qV_m/kT$, $\eta_{c2} = (V_{c2} - V_m)q/kT$ and

13

$$\text{erf}(z) = (2/\pi^{\frac{1}{2}}) \int_{0}^{z} \exp(-u^2) \, du$$

The reduced potential η is dimensionless. Making use of the relation

$$\int d\left(\frac{dV}{dx}\right)^2 = 2 \int \frac{d^2V}{dx^2} \, dV$$

and performing this integration between the bounds V_m and V gives us

$$\left(\frac{dV}{dx}\right)^2 = \frac{1}{q\varepsilon_o} (2\pi kTm)^{\frac{1}{2}} J_s \exp(-\eta_{c1}) \left[h^{\mp}(\eta) + C \, h^{\pm}(\eta) \right] \tag{2.11}$$

where

$$C = \exp(\eta_{c1} - \eta_{c2})$$

$$h^{\pm}(\eta) = \exp(\eta) - 1 \pm 2 \, (\eta/\pi)^{\frac{1}{2}} \mp \exp(\eta) \, \text{erf}(\eta^{\frac{1}{2}})$$

With the help of expression (2.11) the l.f. electric-field strength $E(x)$ can be calculated.

2.2.4 The potential distribution

Let

$$\xi^{\mp} = (x - x_m)/A \tag{2.12}$$

with

$$A = \left[\frac{\varepsilon_o}{qJ_s} \frac{(kT)^{3/2}}{(2m\pi)^{1/2}} \exp(\eta_{c1}) \right]^{\frac{1}{2}}$$

Then (2.11) can be written in the dimensionless form

$$(d\eta/d\xi^{\mp})^2 = h^{\mp}(\eta) + C\ h^{\pm}(\eta)$$

or

$$\xi^{\mp} = \mp \int\limits_{0}^{\eta} dt \left[h^{\mp}(t) + C\ h^{+}_{-}(t) \right]^{-\frac{1}{2}} \tag{2.13}$$

since $\xi^{\mp} = 0$ for $\eta = 0$. It will be readily seen that the potential mini-
mum is situated in the origin of the ξ,η coordinate system (Fig. 2.1). In
the new coordinates the positions of the cathodes are given by ξ_{c1} and
ξ_{c2}.
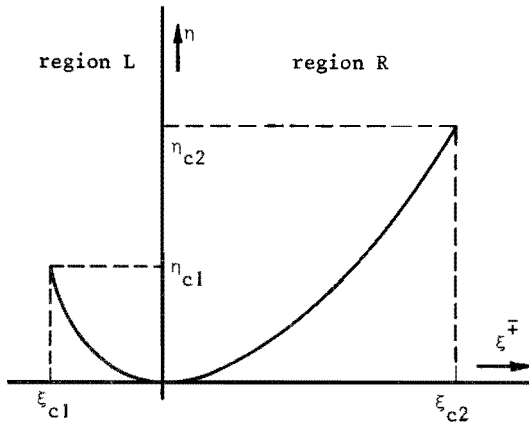
Fig. 2.1 Potential distribution in a double-cathode tube. The position is
given by ξ; ξ is called ξ^{-} in region L and ξ^{+} in region R. The positions
of the cathodes are $\xi^{-} = \xi_{c1}$ and $\xi^{+} = \xi_{c2}$, while η is a reduced potential.

In general, (2.13) cannot be integrated analytically, except in the
particular case[3,4] that the applied d.c. voltage $V = 0$. Then $C = 1$ and

$$\xi^{\mp} = \mp\ 2^{\frac{1}{2}}\ \arctan\{\exp(\eta) - 1\}^{\frac{1}{2}}$$

15

Further, Poisson's equation can then be written in the simple form
(Cf. [5])

$$\frac{d^2\eta}{d\xi^2} = \exp(\eta)$$

This means that the space-charge density depends exponentially on the potential.

2.3 Relation with thermodynamics. Noise.

In this section it is assumed that the cathodes have the same potential. Then the electron cloud is at thermal equilibrium with the cathodes.

The average kinetic energy of the electrons in a volume element at a point x is

$$\tfrac{1}{2} m \int v^2\, n(x,v)\ dv \Big/ \int n(x,v)\ dv$$

The integrations have to be performed over all velocities which can occur at x. Using Eqs.(2.3), (2.5) and (2.6) and remembering that $V_{c2} = 0$ and $\eta_{c1} = \eta_{c2}$ the average kinetic energy turns out to be $\tfrac{1}{2}kT$.[5] This result is in accordance with thermodynamics. Hence, the tube gives off noise that can be calculated with Nyquist's formula. The noise temperature T_n of the tube has to be equal to the temperature of the cathodes.

We observe that the velocity distribution of the electrons at any point x in the inter-electrode space is Maxwellian only when the two cathodes have the same potential.

16

3. ADMITTANCE AND NOISE AT HIGH FREQUENCIES

3.1 Introduction

Consider an arbitrary two-terminal network, which may contain resistors, capacitors, inductors, tubes and transistors. According to a general network theorem, the noise[6] of such a network for the frequency interval df can be described by a noise current generator of zero admittance connected in parallel to an admittance Y (Fig. 3.1).
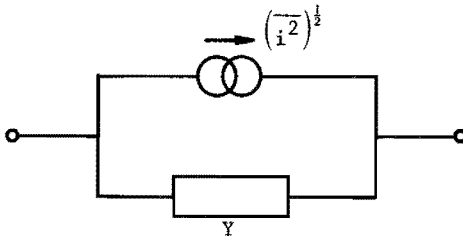
Fig. 3.1. Equivalent circuit of a noisy two-terminal network of admittance Y between the terminals. Its noise is characterised by a noise current generator.

Schwarz, Paucksch[7], Löcherer[8] and Hubert[9] have developed a high-frequency theory for the admittance and the noise of a normal plane space-charge limited diode, including transit-time effects.

In this chapter their theory will be generalised for the double-cathode tube. It turns out that such a tube can be described by a system of two integral equations. Solving this system gives us the h.f. electric-field strength in the inter-electrode space. Then, it is easy to determine the admittance and the noise of the tube. We shall use the theory given in the previous chapter, but now time-dependent quantities have to be introduced.

17

3.2 Derivation of the basic equations

In order to be able to calculate the admittance and the noise of a double-cathode tube the same assumptions have been made as in the case of a normal diode[7,8,9]. These assumptions are:

1. The diode works in the space-charge region.

2. The system is one-dimensional. Movements of the electrons parallel to the emitting surfaces need not be taken into account.

3. The velocity distribution of the emitted electrons is Maxwellian at the surfaces of the cathodes.

4. There are no collisions between electrons.

5. Fluctuations are small enough to allow linearisation of the problem.

Further, it is supposed that the two cathodes are identical as regards the emission and that they have the same temperature.

3.2.1 Total current density. Liouville's law

We obtain the total current density $j_{tot}(t)$ by adding the displacement current density and the convection current density

$$j_{tot}(t) = \varepsilon_o \frac{\partial E(x,t)}{\partial t} + j_c(x,t) \qquad (3.1)$$

The convection current density consists of two parts

$$j_c(x,t) = j_{c1}(x,t) + j_{c2}(x,t) \qquad (3.2)$$

caused by electrons coming from cathode c_1, and from cathode c_2, respectively. We observe that the current densities are chosen positive in the positive x-direction.

The convection current densities can be written in the forms

$$j_{c1}(x,t) = -q \int_{v_{min}(x,t)}^{\infty} n_1(x,v,t) \, v \, dv \qquad (3.3)$$

and

$$j_{c2}(x,t) = q \int_{v_{max}(x,t)}^{-\infty} n_2(x,v,t) \, v \, dv \qquad (3.4)$$

where $v_{min}(x,t)$ is the lowest velocity, in the plane x at time t, of the electrons coming from cathode c_1, and where $n_1(x,v,t)$ is the time-dependent phase-space density of electrons emitted from cathode c_1. Similar definitions hold for $v_{max}(x,t)$ and $n_2(x,v,t)$ with respect to cathode c_2, but v_{max} is now the highest velocity.

When there are no collisions, Liouville's law gives us the following equations

$$\frac{dn_1}{dt} = \frac{\partial n_1}{\partial t} + v \frac{\partial n_1}{\partial x} + b \frac{\partial n_1}{\partial v} = 0 \qquad (3.5)$$

$$\frac{dn_2}{dt} = \frac{\partial n_2}{\partial t} + v \frac{\partial n_2}{\partial x} + b \frac{\partial n_2}{\partial v} = 0 \qquad (3.6)$$

where

$$b = -\frac{q}{m} E(x,t)$$

3.2.2 Linearisation of the above equations

We now split each quantity into its d.c. and a.c. parts. Let

$$n_1(x,v,t) = n_{1d}(x,v) + n_{1a}(x,v,t)$$

$$n_2(x,v,t) = n_{2d}(x,v) + n_{2a}(x,v,t)$$

$$j_{tot}(t) = j_{tot;d} + j_{tot;a}(t)$$

$$E(x,t) = E_d(x) + E_a(x,t)$$

$$v_{min}(x,t) = v_{min;d}(x) + v_{min;a}(x,t)$$

$$v_{max}(x,t) = v_{max;d}(x) + v_{max;a}(x,t)$$

Putting these expressions into the equations (3.1), (3.5) and (3.6), omitting the d.c. parts and linearising, we obtain

$$
j_{tot;a} = \varepsilon_o \frac{\partial E_a}{\partial t} - q \int_{v_{min;d}(x)}^{\infty} n_{1a}(x,v,t)\, v\, dv +
$$

$$
+ q \int_{v_{max;d}(x)}^{-\infty} n_{2a}(x,v,t)\, v\, dv +
$$

$$
+ q\, n_{1d}\left\{x, v_{min;d}(x)\right\} v_{min;d}(x)\, v_{min;a}(x,t) +
$$

$$
- q\, n_{2d}\left\{x, v_{max;d}(x)\right\} v_{max;d}(x)\, v_{max;a}(x,t) \quad (3.7)
$$

$$
\frac{\partial n_{1a}}{\partial t} + v\, \frac{\partial n_{1a}}{\partial x} - \frac{q}{m} E_d(x)\, \frac{\partial n_{1a}}{\partial v} - \frac{q}{m} E_a(x,t)\, \frac{\partial n_{1d}}{\partial v} = 0 \quad\quad (3.8)
$$

$$
\frac{\partial n_{2a}}{\partial t} + v\, \frac{\partial n_{2a}}{\partial x} - \frac{q}{m} E_d(x)\, \frac{\partial n_{2a}}{\partial v} - \frac{q}{m} E_a(x,t)\, \frac{\partial n_{2d}}{\partial v} = 0 \quad\quad (3.9)
$$

If we know $j_{tot;a}$, then we have a system of 3 equations with 5 unknown variables: n_{1a}, n_{2a}, $v_{min;a}$, $v_{max;a}$ and E_a. The corresponding d.c. parts can be calculated with the help of the expressions (2.5), (2.6), (2.7), (2,8) and (2.11).

20

3.2.3 The two lacking equations

In this section two equations will be derived, which express $v_{min;a}(x,t)$ and $v_{max;a}(x,t)$ as a function of the a.c. part of the electric-field strength E_a. The a.c. component $v_{min;a}(x,t)$ is determined as follows. The smallest velocity in the plane x at time t has that electron from cathode c_1 that was in plane $x_m(t_m)$ at time t_m with zero velocity. Here $x_m(t_m)$ is the position of the potential minimum, which of course is time-dependent. For such an electron the following expression is valid

$$\frac{m}{2} v_{min}^2 (x,t) = - q \int_{x_m(t_m)}^{x(t)} E\{z,t(z)\}dz$$

Further, $x_m(t_m)$ can be written as the sum of its d.c. and a.c. components

$$x_m(t_m) = x_{m;d} + x_{m;a}(t_m)$$

Since $E_d(x_{m;d}) = 0$, by linearising the above expression we find

$$v_{min;a}(x,t)\, v_{min;d}(x) = - \frac{q}{m} \int_{x_{m;d}}^{x(t)} E_a\{z,t(z)\}dz \qquad (3.10)$$

The product of $v_{max;a}(x,t)$ and $v_{max;d}(x)$ is given by an equation analogous to (3.10).

3.3 Transformation of the basic equations

3.3.1 Substitution of new variables

In this section the basic equations (3.7), (3.8) and (3.9) will be transformed into more suited expressions. Define, instead of x and v, new variables η (section 2.2.3) and s

$$\eta = \eta(\xi^{\mp}) \tag{3.11}$$

$$s = \eta(\xi^{\mp}) - \frac{mv^2}{2kT} \tag{3.12}$$

There is a one-to-one correspondence between η and ξ, provided it is restricted to one of the regions L and R. However, this is not the case for s and v. We observe that s is an invariant[*] of the motion of an electron under stationary circumstances.

Further, it is assumed that the a.c. components of the various quantities depend harmonically on the time t. Put

$$n_{1a}(x,v,t) = N_1(\eta,s) \exp(j\omega t)$$

$$n_{2a}(x,v,t) = N_2(\eta,s) \exp(j\omega t)$$

$$\tag{3.13}$$

$$E_a(x,t) = F(\xi^{\mp}) \exp(j\omega t)$$

$$j_{tot;a}(t) = J_{tot} \exp(j\omega t) .$$

where ω is the angular frequency of the current density $j_{tot;a}(t)$. Later on we have to integrate F in respect of $\xi^{\mp}$. That is why F is defined in the way given in Eq. (3.13). Then, the following expressions can be obtained.

$$\frac{\partial}{\partial x} = \frac{1}{A} \frac{d\eta}{d\xi^{\mp}} \left(\frac{\partial}{\partial \eta} + \frac{\partial}{\partial s} \right) \tag{3.14}$$

---

[*] Applying the method of Charpit-Lagrange to Eq.(3.8), with $\partial/\partial t = j\omega$, this invariant is easily found. In fact, s is proportional to the total energy of an electron.

$$\frac{\partial}{\partial v} = -\frac{mv}{kT}\frac{\partial}{\partial s}$$

(3.15)

$$\frac{\partial}{\partial t} = j\,\omega$$

3.3.2 The expression for the current density

From (2.5) and (2.7) one can find

$$n_{1d}\{x,v_{min;d}(x)\} = \frac{m}{kTq}\, J_s\, \exp(-n_{c1})$$

Similarly,

$$n_{2d}\{x,v_{max;d}(x)\} = \frac{m}{kTq}\, J_s\, \exp(-n_{c2})$$

The equations (2.7) and (2.8) can be written in the form

$$v_{min;d}(x) = v_{max;d}(x) = \mp\left(\frac{2kT}{m}\,\eta\right)^{\frac{1}{2}}$$

(3.16)

Using equations (3.10) and (3.13), and the above results, (3.7) gives

$$J_{tot} = j\omega\varepsilon_o\, F(\xi^{\mp}) - q \int_{\mp(2kT\eta/m)^{\frac{1}{2}}}^{\infty} N_1(n,s)\, v\, dv +$$

$$+ q \int_{\mp(2kT\eta/m)^{\frac{1}{2}}}^{-\infty} N_2(n,s)\, v\, dv +$$

$$+ \frac{qA}{kT}\, J_s\{\exp(-n_{c2}) - \exp(-n_{c1})\}\times$$

$$\times \int_{0}^{\xi^{\mp}(t)} F(\xi_1)\, \exp\left[j\omega\{t(\xi_1) - t\}\right] d\xi_1$$

(3.17)

23

Here $\omega\{t - t(\xi_1)\}$ is the transit angle of the slowest electron between the planes $\xi = \xi_1$ and $\xi = \xi^{\mp}$. This electron is characterised by $s = 0$.

3.3.3 The equations for the phase-space densities N_1 and N_2

Let

$$n_{1d}(x,v) = n'_{1d}(\eta,v)$$

Then, from Eq.(2.5) it is found that, omitting the prime,

$$\partial n_{1d}(\eta,v)/\partial v = - \frac{mv}{kT} n_{1d}(\eta,v)$$

Using this result in Eq.(3.8) and remembering the definitions (3.13) gives

$$j\omega N_1 + \frac{v}{A} \frac{d\eta}{d\xi^{\mp}} \frac{\partial N_1}{\partial \eta} + \frac{qv}{kT} F(\xi^{\mp})\, n_{1d} = 0 \qquad (3.18)$$

Similarly, the following expression holds

$$j\omega N_2 + \frac{v}{A} \frac{d\eta}{d\xi^{\mp}} \frac{\partial N_2}{\partial \eta} + \frac{qv}{kT} F(\xi^{\mp})\, n_{2d} = 0 \qquad (3.19)$$

Again the upper signs refer to the region L, the lower signs are valid in the region R. The equations (3.18) and (3.19) do not contain the operator $\partial/\partial s$. One can consider them as ordinary differential equations, in which s is a parameter. By solving these equations N_1 and N_2 can be expressed as functions of F.

For each equation a boundary condition is necessary. The boundary conditions are different for the calculation of the admittance (section 3.6) and of the noise temperature (section 3.7).

24

3.4 Solutions of the equations for N_1 and N_2

The linear differential equations (3.18) and (3.19) can be regarded to be of the type

$$\frac{dy}{dx} + P(x)\,y = Q(x)$$

The general solution has the following form

$$y(x) = \exp\left\{-\int_a^x P(x_1)\,dx_1\right\}\left[y(a) + \int_a^x Q(x_1)\,\exp\left\{\int_a^{x_1} P(x_2)\,dx_2\right\}dx_1\right]$$

Before applying it to (3.18) and (3.19), we shall first define transit angles $\alpha^+(\eta,s)$ and $\beta^+(\eta,s)$ for electrons in region R, and transit angles $\alpha^-(\eta,s)$ and $\beta^-(\eta,s)$ for electrons in region L.

3.4.1 The transit angles $\alpha^\pm$ and $\beta^\pm$

Let an electron be in ξ at time $t(\xi)$. This electron travels from ξ_1 to ξ_2 in the transit time $t(\xi_2) - t(\xi_1)$. By definition the corresponding transit angle is the transit time multiplied by the angular frequency. For electrons that can pass the potential minimum, the transit angle between the potential minimum $\xi = 0$ and the point $\xi = \xi^+$ is

$$\alpha^+(\eta,s) = \omega A(m/2kT)^{\frac{1}{2}} \int_0^\eta \frac{d\eta}{(\eta-s)^{\frac{1}{2}}d\eta/d\xi^+} \qquad (s < 0)$$

Similarly, for such electrons in region L,

$$\alpha^-(\eta,s) = -\,\omega A(m/2kT)^{\frac{1}{2}} \int_0^\eta \frac{d\eta}{(\eta-s)^{\frac{1}{2}}d\eta/d\xi^-} \qquad (s < 0)$$

For electrons that cannot pass the potential minimum, the transit angle

$\beta^{\pm}(\eta,s)$ between the turning point, where $\eta = s$, and another point in the inter-electrode space is

$$\beta^{\pm}(\eta,s) = \pm \ \omega A(m/2kT)^{\frac{1}{2}} \int_{s}^{\eta} \frac{d\eta}{(\eta-s)^{\frac{1}{2}} d\eta/d\xi^{\pm}} \qquad (\eta > s > 0)$$

3.4.2 Expressions for N_1 and N_2 in region L

In order to obtain a complete description of $N_1(\eta,s)$ and $N_2(\eta,s)$ one has to distinguish between four cases

(a) electrons emitted by cathode c_1 that reach cathode c_2;

(b) electrons emitted by cathode c_1 that return to c_1;

(c) electrons emitted by cathode c_2 that reach cathode c_1;

(d) electrons emitted by cathode c_2 that return to c_2.

Eq.(3.18) can be written in the form

$$\frac{\partial N_1}{\partial \eta} + \frac{j\omega A}{v \ d\eta/d\xi^{\mp}} N_1 = - \frac{B^-}{d\eta/d\xi^{\mp}} \exp(s) \ F(\xi^{\mp}) \tag{3.20}$$

with

$$B^- = \frac{mA}{(kT)^2} J_s \exp(-\eta_{c1})$$

Case (a). For such electrons $s < 0$ holds. Further, the following expression is valid along the electron path

$$v = \left\{ \frac{2kT}{m} (\eta-s) \right\}^{\frac{1}{2}}$$

In region L the solution of Eq.(3.20) is

$$N_1(\eta,s) = \exp(-jG) \left[N_1(\eta_{c1},s) - B^- \exp(s) \int_{\xi_{c1}}^{\xi^-} F(\xi_1^-) \ \exp(jG_1) \ d\xi_1^- \right] \tag{3.21}$$

26

where

$$G = G(\eta) = \bar{\alpha}(\eta_{c1},s) - \bar{\alpha}(\eta,s) \quad \text{and} \quad G_1 = G(\eta_1)$$

Case (b). Now, $s > 0$. For electrons travelling in the positive direction the velocity v is

$$v = \left\{ \frac{2kT}{m} (\eta-s) \right\}^{\frac{1}{2}}$$

Then the solution of (3.20) is

$$N_1(\eta,s) = \exp(-jH) \left[N_1(\eta_{c1},s) - \bar{B} \exp(s) \int_{\xi_{c1}}^{\bar{\xi}} F(\bar{\xi_1}) \exp(jH_1) \, d\bar{\xi_1} \right] \qquad (3.22)$$

where

$$H = H(\eta) = \bar{\beta}(\eta_{c1},s) - \bar{\beta}(\eta,s) \quad \text{and} \quad H_1 = H(\eta_1)$$

For an electron which is on its way back to cathode c_1, we have to split the integration into two parts: from the cathode c_1 up to the turning point its velocity is

$$v = \left\{ \frac{2kT}{m} (\eta-s) \right\}^{\frac{1}{2}}$$

from the turning point to the point $\xi = \bar{\xi}$ its velocity is

$$v = - \left\{ \frac{2kT}{m} (\eta-s) \right\}^{\frac{1}{2}}$$

Keeping this in mind, the solution of (3.20) is

$$N_1(\eta,s) = \exp(-jL) \left[N_1(\eta_{c1},s) - \bar{B} \exp(s) \times \right.$$

$$\times \left\{ \int_{\xi_{c1}}^{\xi(s)} F(\xi_1^-) \, \exp(jH_1) \, d\xi_1^- + \int_{\xi(s)}^{\xi^-} F(\xi_1^-) \, \exp(jL_1) \, d\xi_1^- \right\} \right] \qquad (3.23)$$

where $L = L(\eta) = \beta^-(\eta_{c1}, s) + \beta^-(\eta, s)$, $L_1 = L(\eta_1)$ and $\xi(s)$ is the value of ξ^- for which $\eta(\xi^-) = s$.

Case_(c). Again the condition $s < 0$ is valid. Further, the velocity of such an electron is

$$v = - \left\{ \frac{2kT}{m} \, (\eta - s) \right\}^{\frac{1}{2}} .$$

Writing Eq.(3.19) in the standard form gives

$$\frac{\partial N_2}{\partial \eta} + \frac{j\omega A}{v \, d\eta/d\xi^{\mp}} \, N_2 = - \frac{B^+}{d\eta/d\xi^{\mp}} \, \exp(s) \, F(\xi^{\mp}) \qquad (3.24)$$

with

$$B^+ = \frac{mA}{(kT)^2} \, J_s \, \exp(-\eta_{c2})$$

In region L the solution of (3.24) is

$$N_2(\eta, s) = \exp(-jM) \left[N_2(\eta_{c2}, s) - B^+ \exp(s) \times \right.$$

$$\left. \times \left\{ \int_{\xi_{c2}}^{0} F(\xi_1^+) \, \exp(jS_1) \, d\xi_1^+ + \int_{0}^{\xi^-} F(\xi_1^-) \, \exp(jM_1) \, d\xi_1^- \right\} \right] \qquad (3.25)$$

where

$$M = M(\eta) = \alpha^+(\eta_{c2}, s) + \alpha^-(\eta, s) \quad \text{and} \quad M_1 = M(\eta_1),$$

$$S = S(\eta) = \alpha^+(\eta_{c2}, s) - \alpha^+(\eta, s) \quad \text{and} \quad S_1 = S(\eta_1).$$

Case_(d). The electrons cannot enter region L.

3.4.3 Expressions for N_1 and N_2 in region R

Similarly, $N_1(\eta,s)$ and $N_2(\eta,s)$ can be calculated in region R. The reason why the results are not given here will become clear later on.

3.5 Integral equations for the field strength F

In this section an integral equation is obtained for the h.f. electric-field strength $F(\xi^{\mp})$ by eliminating $N_1(\eta,s)$ and $N_2(\eta,s)$ from Eq. (3.17). This integral equation is derived for region L. However, it turns out that also terms occur that depend on the field strength $F(\xi^+)$ in region R. These terms are connected with electrons emitted by cathode c_2 that have sufficient energy in order to pass the potential minimum. Their influence on $F(\xi^-)$ in region L depends on their previous history in region R and hence on the field strength $F(\xi^+)$ in that region.

From symmetry considerations another integral equation can be found that is valid in region R.

3.5.1 The transit angle of the slowest electron

Restricting ourselves to region L, the last term of Eq.(3.17) is a function of the transit angle of the slowest electron between the planes $\xi = \xi_1^-$ and $\xi = \xi^-$. It is easy to find

$$\omega\left\{t(\xi_1^-) - t(\xi^-)\right\} = \alpha^-(\eta_1,o) - \alpha^-(\eta,o)$$

where $\eta_1 = \eta(\xi_1^-)$.

3.5.2 The integral equation for F in region L

By using the above result, Eq.(3.17) can be written in the form

29

$$J_{tot} = j\omega\varepsilon_o \, F(\xi^-) - q \int_{-(2kT\eta/m)^{\frac{1}{2}}}^{\infty} N_1 v \, dv + q \int_{-(2kT\eta/m)^{\frac{1}{2}}}^{-\infty} N_2 v \, dv +$$

$$+ (D^+ - D^-) \int_{o}^{\xi^-} F(\xi_1^-) \, \exp\{j\alpha^-(\eta_1,o) - j\alpha^-(\eta,o)\} d\xi_1^- \qquad (3.26)$$

with

$$D^+ = \frac{qA}{kT} J_s \, \exp(-\eta_{c2}) = \frac{qkT}{m} B^+$$

and

$$D^- = \frac{qA}{kT} J_s \, \exp(-\eta_{c1}) = \frac{qkT}{m} B^-$$

The second term of the right-hand member can be expressed as the sum of three integrals (a), (b) and (c)

$$-q \int_{-(2kT\eta/m)^{\frac{1}{2}}}^{0} N_1 v \, dv - q \int_{0}^{(2kT\eta/m)^{\frac{1}{2}}} N_1 v \, dv - q \int_{(2kT\eta/m)^{\frac{1}{2}}}^{\infty} N_1 v \, dv \qquad (3.27)$$

Integral (a) originates from returning electrons on their way back. Since $v \, dv = - \, ds \, kT/m$, it is found that

$$-q \int_{-(2kT\eta/m)^{\frac{1}{2}}}^{0} N_1 v \, dv = \frac{qkT}{m} \int_{o}^{\eta} N_1(\eta,s) \, ds$$

$$= \frac{qkT}{m} \int_{o}^{\eta} N_1(\eta_{c1},s) \, \exp(-jL) \, ds +$$

$$- D^- \int_{o}^{\eta} \exp(s-jL) \, ds \left[\int_{\xi_{c1}}^{\xi(s)} F(\xi_1^-) \, \exp(jH_1) \, d\xi_1^- + \right.$$

$$\left. + \int_{\xi(s)}^{\xi^-} F(\xi_1^-) \, \exp(jL_1) \, d\xi_1^- \right]$$

30

Here Eq.(3.23) has been applied. Now, the order of integration has to be changed in the two repeated integrals (Fig. 3.2). The first repeated integral becomes

$$- D^- \int_{\xi_{cl}}^{\xi^-} F(\xi_1^-) \, d\xi_1^- \int_0^{\eta} \exp(s + jH_1 - jL) \, ds +$$

$$- D^- \int_{\xi^-}^{0} F(\xi_1^-) \, d\xi_1^- \int_0^{\eta_1} \exp(s + jH_1 - jL) \, ds \qquad (3.28)$$

and the second repeated integral

$$+ D^- \int_{\xi^-}^{0} F(\xi_1^-) \, d\xi_1^- \int_0^{\eta_1} \exp(s + jL_1 - jL) \, ds \qquad (3.29)$$
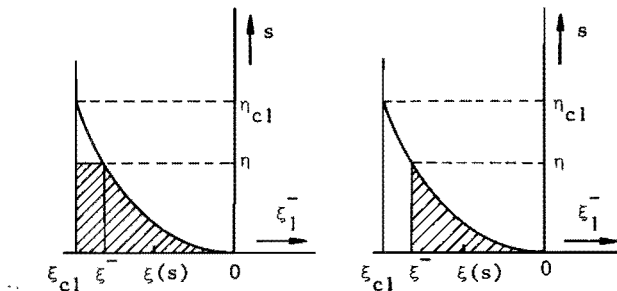
Fig. 3.2. Areas of integration of the integrals (3.28) and (3.29).

Changing the order of integration, the bounds can be read from the figure (Cf.[8]).

Then, the integral (a) is equal to

$$- q \int_{-(2kT\eta/m)^{\frac{1}{2}}}^{0} N_1 \, v \, dv = + \frac{qkT}{m} \int_0^{\eta} N_1(\eta_{cl}, s) \exp(-jL) \, ds +$$

31

$$- D^- \int_{\xi_{c1}}^{\xi^-} F(\xi_1^-) \, d\xi_1^- \int_0^\eta \exp(s + jH_1 - jL) \, ds +$$

$$- D^- \int_{\xi^-}^0 F(\xi_1^-) \, d\xi_1^- \int_0^{\eta_1} \exp(s + jH_1 - jL) \, ds +$$

$$+ D^- \int_{\xi^-}^0 F(\xi_1^-) \, d\xi_1^- \int_0^{\eta_1} \exp(s + jL_1 - jL) \, ds \quad (3.30)$$

Integral (b) is the contribution of returning electrons that are travelling in the positive direction. By using Eq.(3.22) it is not difficult to find that

$$- q \int_0^{(2kT\eta/m)^{\frac{1}{2}}} N_1 \, v \, dv = - \frac{qkT}{m} \int_0^\eta N_1(\eta_{c1},s) \exp(- jH) \, ds +$$

$$+ D^- \int_{\xi_{c1}}^{\xi^-} F(\xi_1^-) \, d\xi_1^- \int_0^\eta \exp(s + jH_1 - jH) \, ds \quad (3.31)$$

Integral (c) is caused by electrons that can pass the potential minimum. With the help of Eq.(3.21) we now obtain

$$- q \int_{(2kT\eta/m)^{\frac{1}{2}}}^\infty N_1 \, v \, dv = \frac{qkT}{m} \int_0^{-\infty} N_1(\eta_{c1},s) \exp(-jG) \, ds +$$

$$- D^- \int_{\xi_{c1}}^{\xi^-} F(\xi_1^-) \, d\xi_1^- \int_0^{-\infty} \exp(s + jG_1 - jG) \, ds \quad (3.32)$$

Next, the third term of the right-hand member of Eq.(3.26) can be expressed as follows

32

$$q \int_{-(2kT\eta/m)^{\frac{1}{2}}}^{-\infty} N_2 \ v \ dv = - \frac{qkT}{m} \int_{o}^{-\infty} N_2(\eta_{c2}, s) \ exp(-jM) \ ds \ +$$

$$+ \ D^+ \int_{o}^{-\infty} exp(s) \ ds \left[\int_{\xi_{c2}}^{o} F(\xi_1^+) \ exp(jS_1 - jM) \ d\xi_1^+ \ + \right.$$

$$\left. + \int_{o}^{\xi^-} F(\xi_1^-) \ exp(jM_1 - jM) \ d\xi_1^- \right]$$

$$= - \frac{qkT}{m} \int_{o}^{-\infty} N_2(\eta_{c2}, s) \ exp(-jM) \ ds \ +$$

$$+ \ D^+ \int_{\xi_{c2}}^{o} F(\xi_1^+) \ d\xi_1^+ \int_{o}^{-\infty} exp(s + jS_1 - jM) \ ds \ +$$

$$+ \ D^+ \int_{o}^{\xi^-} F(\xi_1^-) \ d\xi_1^- \int_{o}^{-\infty} exp(s + jM_1 - jM) \ ds \qquad (3.33)$$

where η_1 and ξ_1^- or ξ_1^+ are corresponding variables. Finally, using (3.27), (3.30),(3.31),(3.32) and (3.33), the expression (3.26) can be written in the following form

$$J_{tot} = j\omega\varepsilon_o \ F(\xi^-) + f(\xi^-) + \int_{\xi_{c1}}^{\xi^-} F(\xi_1^-) \ K_1(\xi^-, \xi_1^-) \ d\xi_1^- \ +$$

$$+ \int_{\xi^-}^{o} F(\xi_1^-) \left\{ K_2(\xi^-, \xi_1^-) + K_3(\xi^-, \xi_1^-) \right\} d\xi_1^- \ +$$

$$+ \int_{o}^{\xi_{c2}} F(\xi_1^+) \ K_4(\xi^-, \xi_1^+) \ d\xi_1^+ \qquad (3.34L)$$

33

with

$$f(\xi^-) = -2j\frac{qkT}{m}\int_0^\eta N_1(\eta_{c1},s)\,\exp\{-j\beta^-(\eta_{c1},s)\}\,\sin\beta^-(\eta,s)\,ds +$$

$$+\frac{qkT}{m}\int_0^{-\infty} N_1(\eta_{c1},s)\,\exp\{j\alpha^-(\eta,s) - j\alpha^-(\eta_{c1},s)\}\,ds +$$

$$-\frac{qkT}{m}\int_0^{-\infty} N_2(\eta_{c2},s)\,\exp\{-j\alpha^-(\eta,s) - j\alpha^+(\eta_{c2},s)\}\,ds$$

$$K_1(\xi^-,\xi_1^-) = 2jD^-\int_0^\eta \exp\{s - j\beta^-(\eta_1,s)\}\,\sin\beta^-(\eta,s)\,ds +$$

$$-D^-\int_0^{-\infty} \exp\{s - j\alpha^-(\eta_1,s) + j\alpha^-(\eta,s)\}\,ds$$

$$K_2(\xi^-,\xi_1^-) = 2jD^-\int_0^{\eta_1} \exp\{s - j\beta^-(\eta,s)\}\,\sin\beta^-(\eta_1,s)\,ds +$$

$$-D^+\int_0^{-\infty} \exp\{s - j\alpha^-(\eta,s) + j\alpha^-(\eta_1,s)\}\,ds$$

$$K_3(\xi^-,\xi_1^-) = -(D^+ - D^-)\,\exp\{j\alpha^-(\eta_1,o) - j\alpha^-(\eta,o)\}$$

$$K_4(\xi^-,\xi_1^+) = -D^+\int_0^{-\infty} \exp\{s - j\alpha^+(\eta_1,s) - j\alpha^-(\eta,s)\}\,ds$$

Eq.(3.34L) is a linear integral equation in $F(\xi^{\mp})$, which is derived for region L. The functions $f(\xi^-)$, $K_1(\xi^-,\xi_1^-)$, $K_2(\xi^-,\xi_1^-)$, $K_3(\xi^-,\xi_1^-)$ and $K_4(\xi^-,\xi_1^+)$ are known, while J_{tot} can be prescribed. In order to obtain a complete description of the double-cathode tube, another integral equation in F has to be found for region R (See the beginning of section 3.5).

3.5.3 The integral equation for F in region R

We shall call the integral equation for F in region R equation
(3.34R). It can be derived from Eq.(3.34L) by applying the following sym-
metry relations

(a) each index + changes into an index -, and vice versa.

(b) N_1 changes into N_2 and vice versa.

(c) η_{c1} changes into η_{c2} and vice versa, except in A, as defined in
Eq.(2.12).

(d) f, K_1, K_2, K_3 and K_4 correspond with -f, $-K_1$, $-K_2$, $-K_3$ and $-K_4$.

3.6 The h.f. admittance

Neglecting the noise and enforcing an a.c. current density J_{tot}
through the tube, the circuit of Fig. 3.1 is simplified to that of Fig.
3.3. Then, the terms $f(\xi^-)$ in Eq.(3.34L) and $f(\xi^+)$ in Eq.(3.34R) are zero,
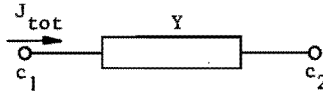
Fig. 3.3. Representation of a double-cathode tube, when the noise is neg-
lected. The enforced a.c. current density is characterised by J_{tot}.

because $N_1(\eta_{c1},s) = N_2(\eta_{c2},s) = 0$. Further, the admittance Y per unit area
is given by

$$Y = J_{tot} \bigg/ \left\{ A \int_{\xi_{c1}}^{\xi_{c2}} F(\xi)\ d\xi \right\}$$

(3.35)

where $F(\xi)$ is found by solving the system of integral equations under the
above conditions.

35

3.7 The h.f. noise

3.7.1 Noise temperature of the double-cathode tube

The noise temperature T_n of any arbitrary two-terminal network is de-fined[6] as the available noise output P_a in a frequency interval Δf, di-vided by $k \Delta f$.

$$T_n = P_a / k \, \Delta f \qquad (3.36)$$

If there is no external current, then between the terminals a noise volt-age $e(t)$ with an r.m.s. value $\left(\overline{e^2} \, \Delta f \right)^{\frac{1}{2}}$ is present and the available power P_a satisfies the following expression

$$P_a = \frac{\overline{e^2(t)} \, \Delta f}{4 \, R} \qquad (3.37)$$

where R is the real part of the impedance Z of the network. From (3.36) and (3.37) it is found that

$$T_n = \overline{e^2(t)} \Big/ 4kR \qquad (3.38)$$

The numerator of Eq.(3.38) is composed of a sum of noise contributions with r.m.s. values $\left(\overline{|e_s|^2} \, ds \right)^{\frac{1}{2}}$, each of which corresponds with a group of electrons emitted by one of the cathodes and having a reduced energy lying between s and s + ds

$$\overline{e^2(t)} = \int_{c1} \overline{|e_s|^2} ds + \int_{c2} \overline{|e_s|^2} ds \qquad (3.39)$$

Here it is assumed that the various terms are uncorrelated with each other, which means that they should be added quadratically.

36

The individual quantities $\overline{|e_s|^2} ds$ are calculated in the following

manner. Suppose there are no fluctuations in the emission of the two

cathodes, except in the group of electrons from cathode c_1 with reduced

energy between s and $s + ds$. Then the distribution of the electric-field

strength $F(\xi^{\mp})$ in the inter-electrode space can be determined from equa-

tions (3.34L) and (3.34R) with $J_{tot} = \bar{0}$, while in $f(\xi^-)$ and $f(\xi^+)$ only

those terms occur that are proportional with $N_1(\eta_{c1}, s)$ ds. Integration of

$F(\xi^{\mp})$ from ξ_{c1} to ξ_{c2} gives the (complex) amplitude which corresponds

with $e_s(ds)^{\frac{1}{2}}$ in the first integral of Eq.(3.39), and is related to a fre-

quency band between f and $f + \Delta f$. Here, implicitly, the theorem is em-

ployed that it is allowed to calculate the response of a circuit to an

input noise signal in terms of complex quantities, provided the band width

concerned is small[6].

Similarly, the noise contribution of electrons emitted by cathode c_2

can be found.

In the sections 3.7.2 and 3.7.3 the noise analysis will be completed

with a calculation of the noise terms in the integral equations (3.34L)

and (3.34R).

3.7.2 The noise terms in the integral equations

For electrons that are emitted by cathode c_1 and have a reduced energy

lying between s and $s + ds$, the noise terms $f(\xi^-)$ and $f(\xi^+)$ occurring in

equations (3.34L) and (3.34R) become

$$f(\xi^-) = \begin{cases} - 2j \, \frac{qkT}{m} \, N_1(\eta_{c1}, s) \, ds \, \exp\{-j\beta^-(\eta_{c1}, s)\} \sin \beta^-(\eta, s) & (0 < s < \eta) \\ 0 & (s \geq \eta) \\ - \frac{qkT}{m} \, N_1(\eta_{c1}, s) \, ds \, \exp\{j\alpha^-(\eta, s) - j\alpha^-(\eta_{c1}, s)\} & (s < 0) \end{cases}$$

37

$$f(\xi^+) = \begin{cases} -\dfrac{qkT}{m} N_1(\eta_{c1},s) \, ds \, \exp\{-j\alpha^+(\eta,s) - j\alpha^-(\eta_{c1},s)\} & (s < 0) \\[12pt] 0 & (s \geq 0) \end{cases}$$

In the above expressions $N_1(\eta_{c1},s) \, ds$ has to be replaced by the r.m.s. value calculated per unit of bandwidth

$$N_1(\eta_{c1},s) \, ds \longrightarrow \left[\overline{\{N_1(\eta_{c1},s) \, ds\}^2}\right]^{\frac{1}{2}}$$

For electrons that are emitted by cathode c_2 and have a reduced energy lying between s and $s + ds$, the corresponding noise terms in the integral equations (3.34L) and (3.34R) become

$$f(\xi^-) = \begin{cases} \dfrac{qkT}{m} N_2(\eta_{c2},s) \, ds \, \exp\{-j\alpha^-(\eta,s) - j\alpha^+(\eta_{c2},s)\} & (s < 0) \\[12pt] 0 & (s \geq 0) \end{cases}$$

$$f(\xi^+) = \begin{cases} 2j \dfrac{qkT}{m} N_2(\eta_{c2},s) \, ds \, \sin \beta^+(\eta,s) \, \exp\{-j\beta^+(\eta_{c2},s)\} & (0<s<\eta) \\[12pt] 0 & (s \geq \eta) \\[12pt] \dfrac{qkT}{m} N_2(\eta_{c2},s) \, ds \, \exp\{j\alpha^+(\eta,s) - j\alpha^+(\eta_{c2},s)\} & (s < 0) \end{cases}$$

Similarly, $N_2(\eta_{c2},s) \, ds$ has to be replaced by

$$\left[\overline{\{N_2(\eta_{c2},s) \, ds\}^2}\right]^{\frac{1}{2}}$$

3.7.3 Mean-square of phase-space densities

Despite the fact that fluctuations in emission actually occur at random over the surfaces of the cathodes, we shall nevertheless suppose

38

that the noise current density in a frequency band from f to f + Δf is uniformly spread over the cathode areas. That this is permissible has been discussed by Thompson[10]. Now restricting our attention to the emission current density dJ_s contributed by electrons emitted by cathode c_1, whose initial velocities lie between v and v + dv, we obtain

$$dJ_s = - q \ n_1(o,v) \ v \ dv$$

$$= - J_s \ \exp(s - \eta_{c1}) \ ds$$

Since dJ_s exhibits shot noise, the theorem of Nyquist for the mean-square fluctuation current density $\overline{dj^2}$ in a bandwidth Δf can be applied[1] (where S is the cathode area):

$$S \ \overline{dj^2} = 2 \ q \left| dJ_s \right| \ \Delta f$$

$$= 2 \ q \ J_s \ \Delta f \ \exp(s - \eta_{c1}) \ ds \qquad (3.40)$$

For the fluctuation dj in the emission current density dJ_s we can also write

$$dj = - q \ \text{Re} \left\{ n_{1a}(o,v,t) \right\} \ v \ dv$$

$$= \frac{qkT}{m} \ \text{Re} \left\{ N_1(\eta_{c1},s) \ \exp(j\omega t) \right\} \ ds$$

Consequently, there is a mean-square fluctuation current density

$$\overline{dj^2} = \tfrac{1}{2} \left(\frac{qkT}{m} \right)^2 \overline{\left\{ N_1(\eta_{c1},s) \ ds \right\}^2} \qquad (3.41)$$

39

Substituting Eq.(3.40) in Eq.(3.41) leads to

$$\overline{\left\{ N_1(\eta_{c1},s) \ ds \right\}^2} = \frac{4}{qS} \left(\frac{m}{kT} \right)^2 J_s \ \exp(s - \eta_{c1}) \ ds \ \Delta f \qquad (3.42)$$

In the same way one can obtain

$$\overline{\left\{ N_2(\eta_{c2},s) \ ds \right\}^2} = \frac{4}{qS} \left(\frac{m}{kT} \right)^2 J_s \ \exp(s - \eta_{c2}) \ ds \ \Delta f \qquad (3.43)$$

3.8 Compatibility of h.f. admittance with l.f. admittance

Let the angular frequency ω tend to zero. Then, supposing the tube to be noise-free, the integral equation (3.34L) changes into

$$J_{tot} = D^- \int_{\xi_{c1}}^{o} F(\xi_1^-) \ d\xi_1^- + D^+ \int_{o}^{\xi_{c2}} F(\xi_1^+) \ d\xi_1^+ \qquad (3.44)$$

for the transit angles of the electrons are all negligible. Doing the same with Eq.(3.34R), one also finds Eq.(3.44). The two integral equations are reduced to one.

Define the a.c. voltage $\phi(\xi)$ by

$$\phi(\xi) = - A \int_{\xi_{c1}}^{\xi} F(y) \ dy$$

Then, Eq.(3.44) can be transformed into

$$J_{tot} = - \frac{q}{kT} J_s \left[\exp(-\eta_{c1}) \ \phi(o) + \exp(-\eta_{c2}) \left\{ \phi(\xi_{c2}) - \phi(o) \right\} \right] \qquad (3.45)$$

Turning now to a low-frequency treatment of the tube, the d.c. current density is (see Fig. 1.1)

$$J = - J_s \ \exp\left(\frac{q}{kT} V_m \right) + J_s \ \exp\left\{ \frac{q}{kT} (V_m - V_{c2}) \right\}$$

40

where J is chosen positive if cathode c_1 has a higher potential than cathode c_2. For the amplitude dJ of slow variations of J we find

$$dJ = - \frac{q}{kT} J_s \left[\exp(-\eta_{c1}) \, dV_m + \exp(-\eta_{c2}) \left\{ dV_{c2} - dV_m \right\} \right] \qquad (3.46)$$

Identifying dJ with $J_{tot} \exp(j\omega t)$, dV_m with $\phi(o) \exp(j\omega t)$, dV_{c2} with $\phi(\xi_{c2}) \exp(j\omega t)$, shows complete correspondence between the equations (3.45) and (3.46). This proves the compatibility of the l.f. and the h.f. theory, as regards the admittance of a double-cathode tube, when ω tends to zero, for the general case that there is a potential difference between the two cathodes.

3.9 Normal diode considered as a special double-cathode tube

In this section the integral equations (3.34L) and (3.34R) for the double-cathode tube will be compared with the integral equations that describe the behaviour of a normal diode at high frequencies[8].

Since a normal plane diode is a double-cathode tube whose second cathode c_2 has no emission, its integral equations are derived by putting

$$N_2(\eta_{c2}, s) = 0$$

and

$$(J_s)_{c2} = 0$$

The latter expression is satisfied, if in the integral equations (3.34L) and (3.34R) D^+ is replaced by zero. It can be shown that then the equations (3.34L) and (3.34R) become identical with Eqs. (17) and (15) of Löcherer[8].

41

3.10 The Fredholm equation of the second kind

Mathematically, the two equations (3.34L) and (3.34R) can be regarded as one integral equation of the form[11]

$$g(\xi) = F(\xi) - \lambda \int_{\xi_{c1}}^{\xi_{c2}} K(\xi,\xi_1) \, F(\xi_1) \, d\xi_1 \qquad (3.47)$$

where $\lambda = -1/j\omega\varepsilon_o$ and the kernel $K(\xi,\xi_1)$ is a bounded continuous function of both variables in the closed square $\xi_{c1} \leq \xi, \xi_1 \leq \xi_{c2}$, except for $\xi_1 = 0$, if $\xi_{c1} \neq - \xi_{c2}$ (Fig. 3.4). On the x-axis the function $K_3(\xi,\xi_1)$ is not defined at all, except in the origin:

$$K_3(o,o) = D^- - D^+$$

Keeping ξ_1 fixed, the real and imaginary parts of $K_3(\xi,\xi_1)$ have the same

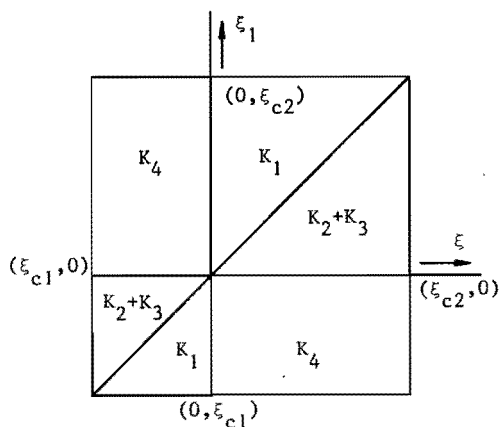

Fig. 3.4. The kernel $K(\xi,\xi_1)$ in the various parts of the closed square $\xi_{c1} \leq \xi, \xi_1 \leq \xi_{c2}$. It is discontinuous on the line $\xi_1 = 0$ $(-\xi_{c1} \neq \xi_{c2})$. The region on the left of $\xi = 0$ corresponds with Eq.(3.34L), that on the right of $\xi = 0$ with Eq.(3.34R).

kind of singularity as the function $f(x) = \sin(1/x)$, when x tends to zero. Physically, this phenomenon corresponds with the infinite transit times of electrons, which have zero velocity in the potential minimum.

If $\xi \leq 0$, then the kernel $K(\xi,\xi_1)$ is given by Eq.(3.34L). If $\xi \geq 0$, the kernel $K(\xi,\xi_1)$ can be found in Eq.(3.34R). Further, $j\omega\varepsilon_o\, g(\xi) =$ $= J_{tot} - f(\xi^-)$ in the first region, and $j\omega\varepsilon_o\, g(\xi) = J_{tot} - f(\xi^+)$ in the second region.

Now, consider the particular case that $-\xi_{c1} = \xi_{c2}$. Then, of course, $\eta_{c1} = \eta_{c2}$, while $K_3 \equiv 0$. It is easy to prove that the function K is symmetric: $K(\xi,\xi_1) = K(\xi_1,\xi)$. Besides, $K(\xi,\xi_1)$ is continuous everywhere in the closed square $-\xi_{c2} \leq \xi,\xi_1 \leq \xi_{c2}$ (Fig. 3.5).
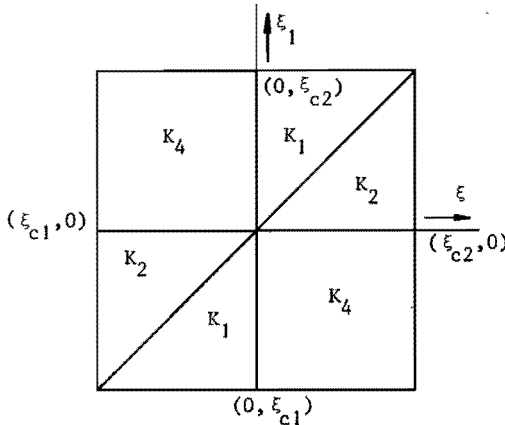

Fig. 3.5. The kernel $K(\xi,\xi_1)$, if $-\xi_{c1} = \xi_{c2}$. It is continuous and symmetric in the closed square $\xi_{c1} \leq \xi,\xi_1 \leq \xi_{c2}$.

The question which arises is: Has Eq.(3.47) in all cases a unique solution? We define an operator P by

$$PF = \int_{\xi_{c1}}^{\xi_{c2}} K(\xi,\xi_1)\, F(\xi_1)\, d\xi_1$$

It can be proved in our case that $K(\xi, \xi_1)$ is an L^2 kernel[12] and that PF is in $C[\xi_{c1}, \xi_{c2}]$, i.e. the space of continuous functions on $[\xi_{c1}, \xi_{c2}]$, whenever F is an element of $L^2(\xi_{c1}, \xi_{c2})$. If the condition for F were not fulfilled, the energy associated with the electric field would be infinite. Then, since $g(\xi)$ is in $C[\xi_{c1}, \xi_{c2}]$, there is a unique solution $F(\xi)$ of Eq.(3.47) that is in $C[\xi_{c1}, \xi_{c2}]$, provided the homogeneous equation derived from Eq.(3.47) only has the trivial solution $F(\xi) \equiv 0$[12]. The uniqueness of the solution $F(\xi)$ was already implicitly used in sections 3.6 and 3.7.

Physically, the solutions of the homogeneous equation which are not trivial may be connected with the occurrence of impedances with negative real parts (Cf.[9]). Then oscillations can take place. Experimentally, such oscillations have been found in normal diodes by Llewellyn and Bowen[13]. In their paper an average transit time of electrons that travel from the cathode to the anode, plays an important part. Whenever this transit angle is equal to $2\pi n + \frac{\pi}{2}$, where $n = 1, 2, 3$, etc., then the electron stream exhibits a negative resistance. However, in the case of the double-cathode tube working in the space-charge region, it seems most improbable that oscillations do exist, because there are two opposite electron streams that do not cooperate.

4. NUMERICAL ANALYSIS OF THE EQUATIONS

4.1 Introduction

Since the integral equations (3.34L) and (3.34R) cannot be solved an-
alytically, a numerical treatment of the problem is needed. To that end,
first, the equations found will be replaced by a complete symmetric sys-
tem of two other equations, which is more suited for the purpose. Next, a
discretisation of the integral equations will be performed. Then, the
problem can be described by a matrix equation. In order to obtain the ma-
trix elements, it is necessary to calculate the potential distribution
and the transit angles $\alpha^{\mp}(\eta,s)$ and $\beta^{\mp}(\eta,s)$. After determining the matrix
elements, the matrix equation will be solved.

4.2 Other forms of the integral equations

Complete symmetry between regions L and R can be obtained by re-
placing ξ^- by $-\xi^-$. The new ξ^- satisfies the relation $\xi^- \geq 0$. We also in-
troduce the current densities J_{tot}^- and J_{tot}^+, where $J_{tot}^{\mp} = \mp J_{tot}$. The po-
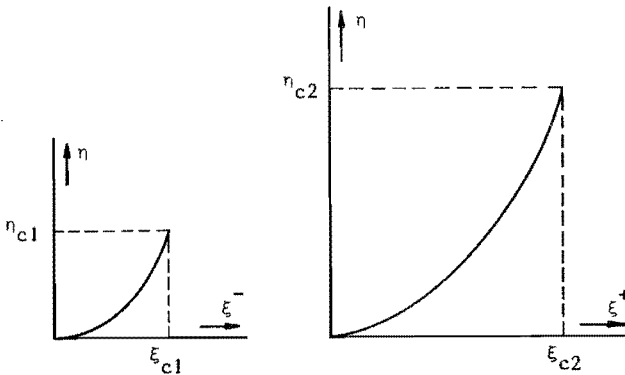tential distributions in both regions are given in Fig. 4.1. Then, the

Fig. 4.1. Potential distribution in a plane space-charge limited double-
cathode tube. In region L the relation $0 \leq \xi^- \leq \xi_{c1}$ is valid. Similarly,
in region R: $0 \leq \xi^+ \leq \xi_{c2}$.

integral equations (3.34L) for region L can be written in the following form:

$$J_{tot}^{-} = j\omega\varepsilon_o \, F(\xi^-) + f(\xi^-) + \int_{\xi_{c1}}^{\xi^-} F(\xi_1^-) \, k_1(\xi^-,\xi_1^-) \, d\xi_1^- +$$

$$+\int_{0}^{\xi^-} F(\xi_1^-) \left\{ k_2(\xi^-,\xi_1^-) + k_3(\xi^-,\xi_1^-) \right\} d\xi_1^- + \int_{0}^{\xi_{c2}} F(\xi_1^+) \, k_4(\xi^-,\xi_1^+) \, d\xi_1^+ \quad (4.1L)$$

with

$$f(\xi^-) = 2j \, \frac{qkT}{m} \int_{0}^{\eta} N_1(\eta_{c1},s) \, \sin \beta^-(\eta,s) \, \exp\{-j\beta^-(\eta_{c1},s)\} \, ds +$$

$$+ \frac{qkT}{m} \int_{0}^{-\infty} N_2(\eta_{c2},s) \, \exp\{-j\alpha^-(\eta,s) - j\alpha^+(\eta_{c2},s)\} \, ds +$$

$$- \frac{qkT}{m} \int_{0}^{-\infty} N_1(\eta_{c1},s) \, \exp\{j\alpha^-(\eta,s) - j\alpha^-(\eta_{c1},s)\} \, ds$$

$$k_1(\xi^-,\xi_1^-) = -2jD^- \int_{0}^{\eta} \sin \beta^-(\eta,s) \, \exp\{s - j\beta^-(\eta_1,s)\} \, ds +$$

$$+ D^- \int_{0}^{-\infty} \exp\{s + j\alpha^-(\eta,s) - j\alpha^-(\eta_1,s)\} \, ds$$

$$k_2(\xi^-,\xi_1^-) = 2jD^- \int_{0}^{\eta_1} \sin \beta^-(\eta_1,s) \, \exp\{s - j\beta^-(\eta,s)\} \, ds +$$

$$- D^+ \int_{0}^{-\infty} \exp\{s - j\alpha^-(\eta,s) + j\alpha^-(\eta_1,s)\} \, ds$$

$$k_3(\xi^-,\xi_1^-) = (D^- - D^+) \, \exp\{j\alpha^-(\eta_1,o) - j\alpha^-(\eta,o)\}$$

46

$$k_4(\xi^-,\xi_1^+) = D^+ \int_0^{-\infty} \exp\{s - j\alpha^-(\eta,s) - j\alpha^+(\eta_1,s)\} \, ds$$

The equivalent form of Eq.(3.34R), which is valid in region R, will be called Eq.(4.1R). It can be derived from Eq.(4.1L) by applying the following symmetry relations:

(a) each index + or - is replaced by - or +

(b) N_1 becomes N_2, and vice versa

(c) η_{c1} changes into η_{c2}, and vice versa.

Further, the new form of the equation for the potential as a function of the position (section 2.2.4) is

$$\frac{d\eta}{d\xi^{\mp}} = \left[h^{\mp}(\eta) + \exp(\eta_{c1} - \eta_{c2}) \, h^{\pm}(\eta) \right]^{\frac{1}{2}} \tag{4.2}$$

with

$$h^{\pm}(\eta) = \exp(\eta) - 1 \pm 2(\eta/\pi)^{\frac{1}{2}} \mp \exp(\eta) \, \mathrm{erf}(\eta^{\frac{1}{2}})$$

Finally, for the transit angles we have, instead of the equations in section 3.4.1

$$\alpha^{\mp}(\eta,s) = \omega A(m/2kT)^{\frac{1}{2}} \int_0^{\eta} \frac{d\eta}{(\eta-s)^{\frac{1}{2}} \, d\eta/d\xi^{\mp}} \quad (s < 0, \; \eta > 0) \tag{4.3}$$

$$\beta^{\mp}(\eta,s) = \omega A(m/2kT)^{\frac{1}{2}} \int_s^{\eta} \frac{d\eta}{(\eta-s)^{\frac{1}{2}} \, d\eta/d\xi^{\mp}} \quad (0 < s < \eta) \tag{4.4}$$

$$A = \left[\frac{\varepsilon_o}{qJ_s} \frac{(kT)^{3/2}}{(2m\pi)^{\frac{1}{2}}} \exp(\eta_{c1}) \right]^{\frac{1}{2}}$$

4.3 Discretisation of the integral equations

The equations (4.1L) and (4.1R) can be solved numerically in the same

way as the following equation

$$\int_a^b k(x,y) \; f(y) \; dy = f(x) + g(x) \tag{4.5}$$

In the pivotal points $x = x_i = a + ih$, where $b = a + nh$ and $i = 0(1)n$, we approximate the integral with the help of the well-known trapezoidal rule. Then, the following equations are obtained

$$h\left\{ \tfrac{1}{2} \, k_{i,o} \, f_o + k_{i,1} f_1 + \ldots + k_{i,n-1} f_{n-1} + \tfrac{1}{2} \, k_{i,n} f_n \right\} = f_i + g_i \tag{4.6}$$

for $i = 0(1)n$, where $k_{i,j} = k(x_i, \; y_j)$; $f_i = f(y_i) = f(x_i)$; $g_i = g(x_i)$. Here, of course, x_i has been chosen equal to y_i. Eq.(4.6) is a set of n+1 linear algebraic equations for the n+1 pivotal values f_i and can be represented by the matrix equation

$$(K - I)f = g \tag{4.7}$$

where I is the identity matrix of the order n+1. If the matrix K - I is regular, there is always a unique solution f of Eq.(4.7). Then we have an approximate solution f of Eq.(4.5) in the points $x = x_i$ with $i = 0(1)n$. It is possible to improve upon the procedure by using a "deferred correction" technique[14], but we did not make use of it.

Applying these general considerations to the equations (4.1L) and (4.1R), we have to choose pivotal values[*] for ξ: In region L as well as

---

[*] In reality we have chosen $\xi_o^{\mp}$ slightly different from zero. The distance between two adjacent points in region L is in general different from the corresponding one in region R.

48

in region R, N+2 equidistant points $\xi_i^{\mp}$ are taken with i = 0(1)N+1, where N

equals, for instance, 9. This means that we have to know the correspond-

ing values of the reduced potential η_i in both regions, together with

the transit angles $\alpha^{\mp}(\eta_i, s)$ and $\beta^{\mp}(\eta_i, s)$.

Then, $k_1(x,y)$, $k_2(x,y)$, $k_3(x,y)$ and $k_4(x,y)$ can be computed in the

discrete points (x_i, y_j), where $x_i \equiv \xi_i^{\mp}$ and $y_j \equiv \xi_{1j}^{\mp}$ with i,j = 0(1)N+1.

It turns out that the equations (4.1L) and (4.1R) are replaced by one ma-

trix equation of the order 2(N+2). Because the matrix elements are com-

plex, this matrix equation is equivalent to a real matrix equation of

the order 4(N+2).

In the following sections the potential distribution and the transit

angles of the electrons will be calculated. We shall return to the matrix

equation in section 4.7.

4.4 Computation of the potential distribution

As stated in the previous section we have only to know the values of

the reduced potentials η_i in the pivotal points $\xi_i^{\mp}$ in the regions L and

R. In order to obtain the potential distribution, Eq.(4.2) has to be

solved. The boundary condition is $\eta = 0$ for $\xi^{\pm} = 0$. In addition,

$\eta_{c1} - \eta_{c2}$ has a prescribed value. In fact, this means that there are two

differential equations which have to be solved simultaneously (See Fig.

4.1). The integration of Eq.(4.2) has been performed by using a Runge-

Kutta method, for which a subroutine RK_1 is available[15]. Since $d\eta/d\xi^{\mp}=0$

for $\xi^{\mp} = 0$, the method of Runge-Kutta fails, when $\xi^{\mp} = 0$ is chosen as a

starting point. Therefore, it is necessary to begin the integration at a

point $\xi^{\pm} = a$, where a equals, for instance, 0.01. The value of η, corre-

sponding with $\xi^{\pm} = a$, can be calculated by means of a Taylor expansion.

With this value of η the Runge-Kutta method was started. In order to sat-

isfy the condition that $\eta_{c1} - \eta_{c2}$ had a fixed value, the integration of Eq. (4.2) was performed iteratively. A typical potential distribution is shown in Fig. 4.2.
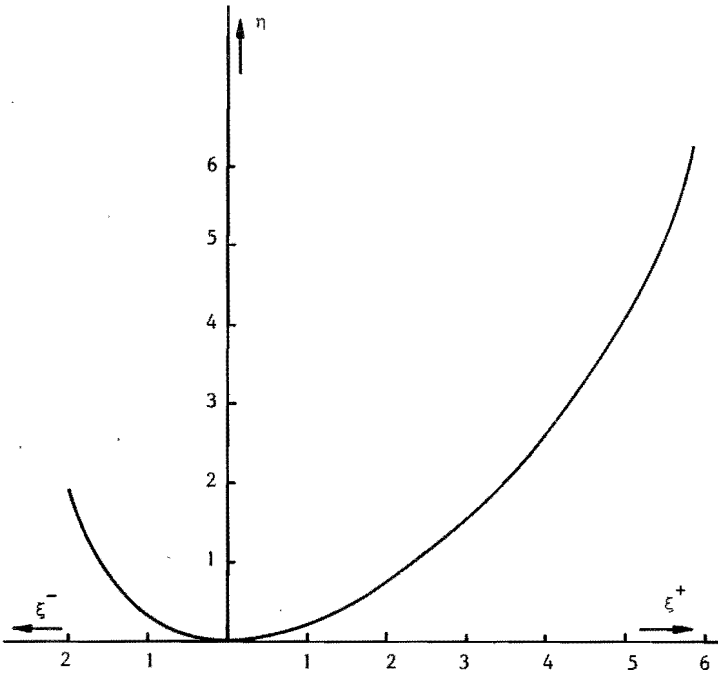
Fig. 4.2. Reduced potential η vs. reduced position $\xi^{\mp}$. Positions of cathodes c_1 and c_2 are $\xi_{c1} = 1.986$ and $\xi_{c2} = 5.837$. Reduced potentials of cathodes c_1 and c_2 are $\eta_{c1} = 1.928$ and $\eta_{c2} = 6.222$.

4.5 Computation of the transit angles

The transit angles for a normal plane diode have been calculated by Paucksch[16]. We have generalised his method for the case of a double-cathode tube. Equations (4.3) and (4.4) contain singular integrals of the type treated by Isaacson and Keller[17]. Further, it is no restriction to

50

suppose $\eta_{c1} - \eta_{c2} \leq 0$. From now on we shall always make this supposition.

It has been pointed out in section 4.3 that we have to know the transit angles $\alpha^{\mp}(\eta,s)$ and $\beta^{\mp}(\eta,s)$, for fixed values η_i, as functions of the reduced energy s. It is, therefore, important to try to find, whenever possible, polynomials in s (with coefficients depending on η) that are good approximations for the transit angles α and β.

Let

$$H^{\mp}(t) = h^{\mp}(t) + \exp(\eta_{c1} - \eta_{c2}) \, h^{\pm}(t)$$

Using Eq.(4.2), the equations (4.3) and (4.4) can be written in the following forms

$$\alpha^{\mp}(\eta,s) = \omega A(m/2kT)^{\frac{1}{2}} \int_{0}^{\eta} \frac{dt}{(t-s)^{\frac{1}{2}}\{H^{\mp}(t)\}^{\frac{1}{2}}} \qquad (s < 0, \ \eta > 0) \qquad (4.8)$$

$$\beta^{\mp}(\eta,s) = \omega A(m/2kT)^{\frac{1}{2}} \int_{s}^{\eta} \frac{dt}{(t-s)^{\frac{1}{2}}\{H^{\mp}(t)\}^{\frac{1}{2}}} \qquad (0 < s < \eta) \qquad (4.9)$$

Clearly, the integrand in Eq.(4.8) is singular for $t = 0$, since $H^{\mp}(t) = O(t)$, when t tends to zero. The integrand in Eq.(4.9) is singular for $t = s$. Moreover, both expressions are divergent, when $s = 0$. This corresponds with the infinite transit times of electrons that can just reach the potential minimum.

4.5.1 Transit angles of electrons that pass the potential minimum

A direct numerical integration of Eq.(4.8) is not possible, owing to the singularity of the integrand at $t = 0$. Let δ be a small positive constant (e.g. $\delta = 0.2$). Several cases of integration can be distinguished, depending on the values of η and s:

(a) η is smaller than δ

(b) η is larger than δ

(c) η is smaller than $|s|/5$

(d) η is larger than $|5s|$.

In case (a), an analytical expression for $\alpha^{\mp}(\eta,s)$ can be derived. It turns out that the normal case of integration treated in (b) can be accelerated for the special cases (c) and (d).

Case (a). Putting $t = y^2$ into Eq.(4.8) gives the following expression

$$\alpha^{\mp}(\eta,s) = \omega A(2m/kT)^{\frac{1}{2}} \int_{0}^{\eta^{\frac{1}{2}}} \frac{dy}{(y^2-s)^{\frac{1}{2}}} \frac{y}{\{H^{\mp}(y^2)\}^{\frac{1}{2}}} \tag{4.10}$$

For small values of y we have, with $C = \exp(\eta_{c1} - \eta_{c2})$,

$$\frac{y}{\{H^{\mp}(y^2)\}^{\frac{1}{2}}} = \frac{1}{(1+C)^{\frac{1}{2}}} (1 + b_1 y + b_2 y^2 + b_3 y^3) \tag{4.11}$$

with

$$b_1 = \mp \frac{2}{3\pi^{\frac{1}{2}}} \frac{1-C}{1+C}$$

$$b_2 = -\frac{1}{4} + \frac{2}{3\pi} \left(\frac{1-C}{1+C}\right)^2$$

$$b_3 = \pm \frac{7}{30\pi^{\frac{1}{2}}} \frac{1-C}{1+C} \pm 20\left(\frac{1}{3\pi^{\frac{1}{2}}} \frac{1-C}{1+C}\right)^3$$

If η is less than δ, integration of (4.10) with the help of Eq.(4.11) leads to

52

$$\alpha^{\mp}(\eta,s) = \omega A \left\{ \frac{2m}{kT(1 + C)} \right\}^{\frac{1}{2}} \left[(1 + b_2 \, s/2)\left\{ \ln\{\eta^{\frac{1}{2}} + (\eta-s)^{\frac{1}{2}}\} - \ln(-s)^{\frac{1}{2}} \right\} + \right.$$

$$+ (b_1 + b_3 s) \left\{ (\eta-s)^{\frac{1}{2}} - (-s)^{\frac{1}{2}} \right\} + (b_2/2)\eta^{\frac{1}{2}}(\eta-s)^{\frac{1}{2}} +$$

$$\left. + (b_3/3) \left\{ (\eta-s)^{3/2} - (-s)^{3/2} \right\} \right] \qquad (4.12)$$

Case (b). If $\eta > \delta$, the integral in Eq.(4.10) has to be split into two parts, one from zero to $\delta^{\frac{1}{2}}$ and the other from $\delta^{\frac{1}{2}}$ to $\eta^{\frac{1}{2}}$. The first part can be calculated by means of Eq.(4.12), while in the second part the exact expression for $H^{\mp}(y^2)$ has to be used.

Case (c). If $\eta < |s|/5$ we have in the whole integration interval of Eq.(4.8)

$$(t-s)^{-\frac{1}{2}} = (-s)^{-\frac{1}{2}} \left(1 + \frac{1}{2}\frac{t}{s} + \frac{3}{8}\frac{t^2}{s^2} + \frac{5}{16}\frac{t^3}{s^3} + \cdots \right)$$

Then, $\alpha^{\mp}(\eta,s)$ can be approximated by

$$\alpha^{\mp}(\eta,s) = \omega A (m/2kT)^{\frac{1}{2}}(-s)^{\frac{1}{2}} \left\{ \xi^{\mp} + \frac{1}{2s} P_1^{\mp}(\eta) + \frac{3}{8s^2} P_2^{\mp}(\eta) + \frac{5}{16s^3} P_3^{\mp}(\eta) \right\} \quad (4.13)$$

with

$$P_n^{\mp}(\eta) = \int_0^{\eta} \frac{t^n}{\{H^{\mp}(t)\}^{\frac{1}{2}}} \, dt = 2 \int_0^{\eta^{\frac{1}{2}}} \frac{y^{2n+1}}{\{H^{\mp}(y^2)\}^{\frac{1}{2}}} \, dy \quad (n = 1,2,3)$$

where again a new variable $y = t^{\frac{1}{2}}$ is introduced. If $\eta \leq \delta$, it is easy to find, using Eq.(4.11), that

$$P^{\mp}(\eta) = \frac{2}{(1+C)^{\frac{1}{2}}} \int_0^{\eta^{\frac{1}{2}}} (1 + b_1 y + b_2 y^2 + b_3 y^3) \, y^{2n} \, dy$$

If $\eta > \delta$, we have

$$P_n^{\mp}(\eta) = \frac{2}{(1+C)^{\frac{1}{2}}} \int_o^{\delta^{\frac{1}{2}}} (1 + b_1 y + b_2 y^2 + b_3 y^3) \, y^{2n} \, dy + 2 \int_{\delta^{\frac{1}{2}}}^{\eta^{\frac{1}{2}}} dy \, \frac{y^{2n+1}}{\{H^{\mp}(y^2)\}^{\frac{1}{2}}}$$

Once the auxiliary functions $P_n^{\mp}(\eta)$ have been calculated for fixed values of η, the transit angles $\alpha^{\mp}(\eta,s)$ can be computed rapidly by means of Eq.(4.13), provided $|s| > 5\eta$.

Case (d). If $\eta > |5s|$, we make use of the following Taylor series expansion

$$(t-s)^{-\frac{1}{2}} = t^{-\frac{1}{2}} \left(1 + \frac{1}{2} \frac{s}{t} + \frac{3}{8} \frac{s^2}{t^2} + \frac{5}{16} \frac{s^3}{t^3} + \dots \right) \tag{4.14}$$

This expansion is applied, if t satisfies the condition

$$t \geq \eta_i \geq \max(M, -5s)$$

where η_i is the value of η that corresponds with one of the pivotal values $\xi_i^{\mp}$ with $i = 0(1)N+1$, and M is a positive number. A possible value of M is 0.5. It turns out that M cannot be chosen too small (see below). Now, the following expression for $\alpha^{\mp}$ is obtained:

$$\alpha^{\mp}(\eta,s) = \alpha^{\mp}(\delta,s) + \omega A (2m/kT)^{\frac{1}{2}} \int_{\delta^{\frac{1}{2}}}^{\eta_i^{\frac{1}{2}}} dy \, \frac{1}{(y^2-s)^{\frac{1}{2}}} \frac{y}{\{H^{\mp}(y^2)\}^{\frac{1}{2}}} +$$

$$+ \omega A (m/2kT)^{\frac{1}{2}} \int_{\eta_i}^{\eta} \frac{dt}{(t-s)^{\frac{1}{2}} \{H^{\mp}(t)\}^{\frac{1}{2}}} \tag{4.15}$$

The second term of the right-hand member of Eq.(4.15) is calculated with the help of the exact expression for $H^{\mp}(y^2)$. A good approximation for the integral in the last term is

54

$$\int_{\eta_i}^{\eta} \frac{dt}{(t-s)^{\frac{1}{2}}\{H^{\mp}(t)\}^{\frac{1}{2}}} = Q_0(\eta) + \frac{1}{2} s \, Q_1(\eta) + \frac{3}{8} s^2 \, Q_2(\eta) + \frac{5}{16} s^3 \, Q_3(\eta)$$

where

$$Q_n(\eta) = \int_{\eta_i}^{\eta} \frac{dt}{t^{n+\frac{1}{2}}\{H^{\mp}(t)\}^{\frac{1}{2}}} \qquad \text{(with } n = 0(1)3),$$

provided $Q_3(\eta)$ is of the same order as $Q_0(\eta)$. Because the integrands of these integrals are singular for $t = 0$, the lower bound η_i has to be chosen not too small. This explains our choice of M. Of course, it is ad-
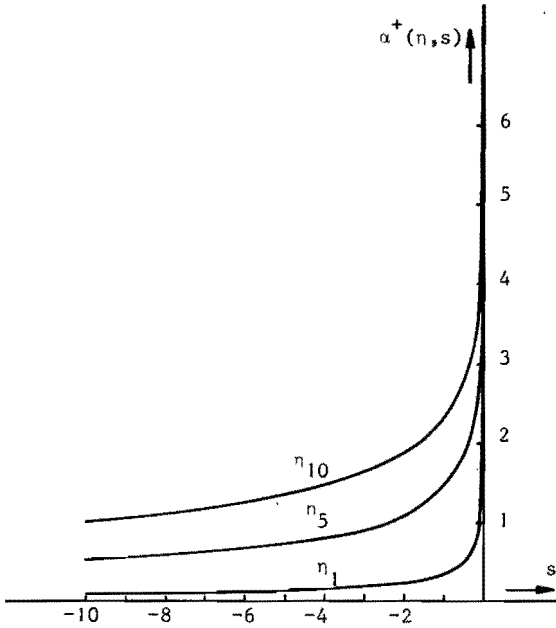

Fig. 4.3. Transit angle $\alpha^+(\eta,s)$ vs. reduced energy s. Frequency 3 GHz, temperature of cathodes 1350°K, saturation current density 0.990 A/cm^2. Reduced potentials of cathodes c_1 and c_2 are $\eta_{c1} = 1.928$ and $\eta_{c2} = 6.222$; $\eta_1 = 0.0786$, $\eta_5 = 1.5130$, $\eta_{10} = 6.222$.

vantageous to compute beforehand the auxiliary functions $Q_n(\eta)$ for fixed values of η.

As an example, transit angles $\alpha^+(\eta,s)$ are plotted as a function of s in Fig. 4.3, where η is a parameter.

4.5.2 Transit angles of returning electrons

The numerical integration of Eq.(4.9) presents difficulties due to the singularity of the integrand at $t = s$. Let again δ be a small positive constant. Several cases will be analysed:

(a) η and s are larger than δ

(b) η is smaller than δ

(c) δ lies in the integration interval (s,η)

(d) η is larger than 5s and $\delta < s$.

(e) η is larger than 5s, but δ lies in (s,η)

(f) η is nearly equal to s, while η is not near zero.

In case (a), the normal procedure of numerical integration has to be applied. In case (b), an analytical expression for $\beta^{\mp}(\eta,s)$ can be derived. Case (c) is a combination of (a) and (b). In the last three cases the numerical integration can be accelerated.

Case (a). Introduce a new variable $y = (t-s)^{\frac{1}{2}}$. Then Eq.(4.9) can be written in the following form

$$\beta^{\mp}(\eta,s) = \omega A (2m/kT)^{\frac{1}{2}} \int_0^{(\eta-s)^{\frac{1}{2}}} \frac{dy}{\{H^{\mp}(y^2+s)\}^{\frac{1}{2}}}$$

The numerical integration has to be performed by employing the exact expression of $H^{\mp}(t)$.

Case (b). Substituting $t = y^2$ in Eq.(4.9) leads to

$$\beta^{\mp}(\eta,s) = \omega A (2m/kT)^{\frac{1}{2}} \int_{s^{\frac{1}{2}}}^{\eta^{\frac{1}{2}}} dy \frac{1}{(y^2-s)^{\frac{1}{2}}} \frac{y}{\{H^{\mp}(y^2)\}^{\frac{1}{2}}}$$

56

When $\eta \leq \delta$, the integrand of this equation can be simplified by using Eq. (4.11). A straightforward calculation shows that then

$$\bar{\beta}^{\mp}(\eta,s) = \omega A \left\{\frac{2m}{kT(1+C)}\right\}^{\frac{1}{2}} \left[(1 + b_2 s/2) \left\{ \ln\{\eta^{\frac{1}{2}} + (\eta-s)^{\frac{1}{2}}\} - \ln(s^{\frac{1}{2}}) \right\} \right.$$

$$\left. + (b_1 + b_3 s + b_2 \eta^{\frac{1}{2}}/2) (\eta-s)^{\frac{1}{2}} + (b_3/3) (\eta-s)^{3/2} \right] \qquad (4.16)$$

Case(c). The integration of Eq.(4.9) is here split into two parts, one from s to δ and the other from δ to η. Putting $t-s = y^2$ in the second part, we obtain

$$\bar{\beta}^{\mp}(\eta,s) = \bar{\beta}^{\mp}(\delta,s) + \omega A (2m/kT)^{\frac{1}{2}} \int_{(\delta-s)^{\frac{1}{2}}}^{(\eta-s)^{\frac{1}{2}}} \frac{dy}{\{\bar{H}^{\mp}(y^2+s)\}^{\frac{1}{2}}} \qquad (4.17)$$

The first term $\bar{\beta}^{\mp}(\delta,s)$ is calculated by means of Eq.(4.16), while the normal numerical integration has to be applied to the second term, if η is not large enough. This condition will be made clear below.

Case (d). Suppose $\eta > \eta_i \geq \max(5s,M)$ and $\eta_{i-1} < \max(5s,M)$. Again, the integration of Eq.(4.9) is performed in two steps, one from s to η_i and the other from η_i to η

$$\bar{\beta}^{\mp}(\eta,s) = \omega A (m/2kT)^{\frac{1}{2}} \left[2 \int_0^{(\eta_i-s)^{\frac{1}{2}}} \frac{dy}{\{\bar{H}^{\mp}(y^2+s)\}^{\frac{1}{2}}} + Q_0(\eta) + \frac{1}{2} s Q_1(\eta) + \right.$$

$$\left. + \frac{3}{8} s^2 Q_2(\eta) + \frac{5}{16} s^3 Q_3(\eta) \right] \qquad (4.18)$$

where some results, obtained previously in the corresponding case for α, have been used.

Case (e). Supposing $\eta > \eta_i \geq \max(5s,M)$ and $\eta_{i-1} < \max(5s,M)$, we have to split the integration into three parts

57

$$\beta^{\mp}(\eta,s) = \omega A(m/2kT)^{\frac{1}{2}} \left(\int_s^\delta + \int_\delta^{\eta_i} + \int_{\eta_i}^\eta\right) \frac{dt}{(t-s)^{\frac{1}{2}}\{H^{\mp}(t)\}^{\frac{1}{2}}} \tag{4.19}$$

Comparing this with the equations (4.16), (4.17) and (4.18), the further treatment of Eq.(4.19) is self-evident.

Case (f). If $\eta-s \leq a$, where a = say 0.01, the transit angle $\beta^{\mp}(\eta,s)$ can be expressed as a series in $\eta-s$. Eq.(4.9) can be written in the following form

$$\beta^{\mp}(\eta,s) = \omega A(m/2kT)^{\frac{1}{2}} \int_{s-\eta}^0 \frac{dy}{(y+\eta-s)^{\frac{1}{2}}\{H^{\mp}(y+\eta)\}^{\frac{1}{2}}}$$

Expanding $\{H^{\mp}(y+\eta)\}^{-\frac{1}{2}}$ in a Taylor series in y, followed by integration, it is found that

$$\beta^{\mp}(\eta,s) = \omega A(m/2kT)^{\frac{1}{2}} (\eta-s)^{\frac{1}{2}} \Big\{ G_1(\eta) + G_2(\eta)\ (\eta-s) +$$

$$+ G_3(\eta)\ (\eta-s)^2 + G_4(\eta)\ (\eta-s)^3 \Big\} \tag{4.20}$$

with

$$G_1(\eta) = 2\{H^{\mp}\}^{-\frac{1}{2}}$$

$$G_2(\eta) = \frac{2}{3}\{H^{\mp}\}^{-3/2} \frac{dH^{\mp}}{d\eta}$$

$$G_3(\eta) = \frac{2}{5}\{H^{\mp}\}^{-5/2}\left(\frac{dH^{\mp}}{d\eta}\right)^2 - \frac{4}{15}\{H^{\mp}\}^{-3/2} \frac{d^2H^{\mp}}{d\eta^2}$$

$$G_4(\eta) = \frac{2}{7}\{H^{\mp}\}^{-7/2}\left(\frac{dH^{\mp}}{d\eta}\right)^3 - \frac{12}{35}\{H^{\mp}\}^{-5/2} \frac{dH^{\mp}}{d\eta}\frac{d^2H^{\mp}}{d\eta^2} +$$

$$+ \frac{8}{105}\{H^{\mp}\}^{-3/2} \frac{d^3H^{\mp}}{d\eta^3}$$

Here $H^{\mp} = H^{\mp}(\eta)$, $dH^{\mp}/d\eta = dH^{\mp}(\eta)/d\eta$, etc. When η is too small, the coefficients $G_1(\eta)$, $G_2(\eta)$, $G_3(\eta)$ and $G_4(\eta)$ are very large. That is why Eq.

58

(4.20) is only a good approximation for $\beta^{\mp}(\eta,s)$, if η is far away from zero, e.g. $\eta > 0.2$. Paucksch[16] has found for the normal diode a power series in $(\eta-s)^{\frac{1}{2}}$, analogous to Eq.(4.20), but with coefficients depending on s.

In Fig. 4.4 results are given for $\beta^{+}(\eta,s)$ plotted against the reduced energy s. Observe that the derivative of β^{+} is infinite in the turning points, where $\eta = s$.
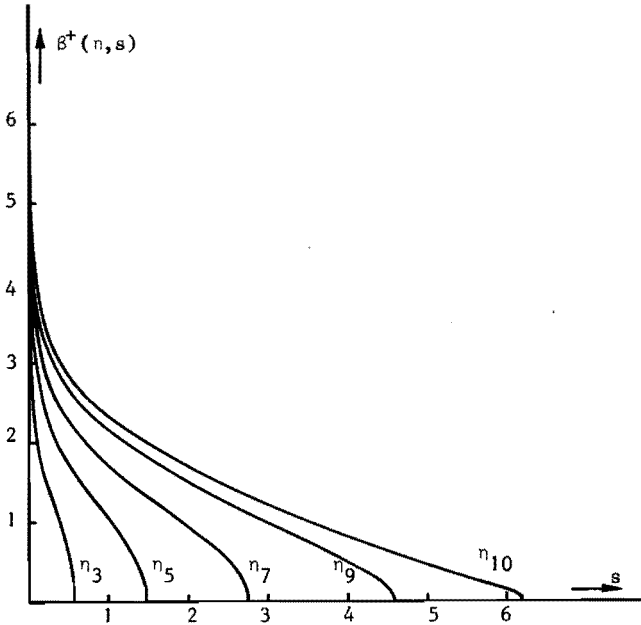

Fig. 4.4. Transit angle $\beta^{+}(\eta,s)$ vs. reduced energy s. The parameter values are the same as in Fig. 4.3. In addition, $\eta_3 = 0.6073$, $\eta_7 = 2.7675$, $\eta_9 = 4.5982$.

4.6 The kernels of the integral equations

4.6.1 Introduction

The results obtained in the previous section enable us to tabulate the transit angles $\alpha^{\mp}(\eta,s)$ and $\beta^{\mp}(\eta,s)$ as a function of s for $2(N+2)$ fixed values of η.

Now, the real and imaginary parts of k_1, k_2, k_3 and k_4 are given below. If $0 < \eta \leq \eta_1$, k_1 is:

$$\text{Re } k_1(\xi^{\mp}, \xi_1^{\mp}) = D^{\mp}\left[\int_0^{\eta} ds \; \exp(s) \; \cos\{\beta^{\mp}(\eta,s) + \beta^{\mp}(\eta_1,s)\} + \right.$$

$$- \int_0^{\eta} ds \; \exp(s) \; \cos\{\beta^{\mp}(\eta,s) - \beta^{\mp}(\eta_1,s)\} +$$

$$\left. + \int_0^{-\infty} ds \; \exp(s) \; \cos\{\alpha^{\mp}(\eta,s) - \alpha^{\mp}(\eta_1,s)\} \right]$$

$$\text{Im } k_1(\xi^{\mp},\xi_1^{\mp}) = D^{\mp}\left[- \int_0^{\eta} ds \; \exp(s) \; \sin\{\beta^{\mp}(\eta,s) + \beta^{\mp}(\eta_1,s)\} + \right.$$

$$- \int_0^{\eta} ds \; \exp(s) \; \sin\{\beta^{\mp}(\eta,s) - \beta^{\mp}(\eta_1,s)\} +$$

$$\left. + \int_0^{-\infty} ds \; \exp(s) \; \sin\{\alpha^{\mp}(\eta,s) - \alpha^{\mp}(\eta_1,s)\} \right]$$

If $0 < \eta_1 \leq \eta$, $k_2 + k_3$ is:

$$\text{Re } k_2(\xi^{\mp},\xi_1^{\mp}) = D^{\mp}\left[- \int_0^{\eta_1} ds \; \exp(s) \; \cos\{\beta^{\mp}(\eta_1,s) + \beta^{\mp}(\eta,s)\} + \right.$$

$$\left. + \int_0^{\eta_1} ds \; \exp(s) \; \cos\{\beta^{\mp}(\eta_1,s) - \beta^{\mp}(\eta,s)\} \right] +$$

$$- D^{\mp} \int_0^{-\infty} ds \, \exp(s) \, \cos\left\{\alpha^{\mp}(\eta,s) - \alpha^{\mp}(\eta_1,s)\right\}$$

$$\text{Im } k_2(\xi^{\mp},\xi_1^{\mp}) = D^{\mp}\left[\int_0^{\eta_1} ds \, \exp(s) \, \sin\left\{\beta^{\mp}(\eta_1,s) + \beta^{\mp}(\eta,s)\right\} + \right.$$

$$\left. + \int_0^{\eta_1} ds \, \exp(s) \, \sin\left\{\beta^{\mp}(\eta_1,s) - \beta^{\mp}(\eta,s)\right\}\right] +$$

$$+ D^{\pm} \int_0^{-\infty} ds \, \exp(s) \, \sin\left\{\alpha^{\mp}(\eta,s) - \alpha^{\mp}(\eta_1,s)\right\}$$

$$\text{Re } k_3(\xi^{\mp},\xi_1^{\mp}) = (D^{\mp}-D^{\pm}) \, \cos\left\{\alpha^{\mp}(\eta_1,o) - \alpha^{\mp}(\eta,o)\right\}$$

$$\text{Im } k_3(\xi^{\mp},\xi_1^{\mp}) = (D^{\mp}-D^{\pm}) \, \sin\left\{\alpha^{\mp}(\eta_1,o) - \alpha^{\mp}(\eta,o)\right\}$$

If $0 < \eta_1$ and $0 < \eta$, k_4 is:

$$\text{Re } k_4(\xi^{\mp},\xi_1^{\pm}) = D^{\pm} \int_0^{-\infty} ds \, \exp(s) \, \cos\left\{\alpha^{\mp}(\eta,s) + \alpha^{\pm}(\eta_1,s)\right\}$$

$$\text{Im } k_4(\xi^{\mp},\xi_1^{\pm}) = - D^{\pm} \int_0^{-\infty} ds \, \exp(s) \, \sin\left\{\alpha^{\mp}(\eta,s) + \alpha^{\pm}(\eta_1,s)\right\}$$

4.6.2 The function k_3

According to Eq.(4.8) we have, if $0 < \eta_1 \leq \eta$,

$$\alpha^{\mp}(\eta_1,o) - \alpha^{\mp}(\eta,o) = - \omega A(m/2kT)^{\frac{1}{2}} \int_{\eta_1}^{\eta} \frac{dt}{t^{\frac{1}{2}}\left\{H^{\mp}(t)\right\}^{\frac{1}{2}}} \tag{4.21}$$

If η satisfies the condition $\eta \leq \delta$, one can find, by expanding $\left\{H^{\mp}(t)\right\}^{-\frac{1}{2}}$ in a Taylor series and integrating,

$$\alpha^{\mp}(\eta_1,o) - \alpha^{\mp}(\eta,o) = - \omega A \left\{ \frac{m}{2kT(1+C)} \right\}^{\frac{1}{2}} \left\{ \ln(\eta/\eta_1) + 2 b_1(\eta^{\frac{1}{2}} - \eta_1^{\frac{1}{2}}) + \right.$$

$$\left. + b_2(\eta - \eta_1) + (2/3) b_3(\eta^{3/2} - \eta_1^{3/2}) \right\}$$

If η and η_1 satisfy the condition $\eta_1 < \delta < \eta$, the integration of Eq.(4.21) has to be done in two steps, one from η_1 to δ and the other from δ to η. The first part is calculated by means of the previous formula with η replaced by δ. In the second part we substitute $y = t^2$, after which its numerical integration is performed. If η is larger than δ, the integration of Eq.(4.21) has to be done in an ordinary numerical way. By means of these results it is not difficult to compute the function k_3.

4.6.3 The functions k_1, k_2 and k_4

Integrals over infinite intervals occur in the functions $k_1(\xi^{\mp},\xi_1^{\mp})$, $k_2(\xi^{\mp},\xi_1^{\mp})$ and $k_4(\xi^{\mp},\xi_1^{\pm})$. For instance, the integral

$$\int_o^{-\infty} ds \, \exp(s) \, \cos\left\{ \alpha^{\mp}(\eta,s) - \alpha^{\mp}(\eta_1,s) \right\}$$

is approximated by replacing the bound $-\infty$ by a finite value b. Because of the exponential behaviour of the integral it is sufficient to choose $b = - 10$.

Further, all the integrals occurring in k_1, k_2 and k_4 have singular integrands in the neighbourhood of $s = 0$. In other words, we always have to start the integration in a point ε away from the point $s = 0$. $|\varepsilon|$ can be taken equal to e.g. 0.01. Thanks to the strongly oscillating character of each of the integrands, the contribution over the interval (o,ε) is not large. On the other hand, their oscillating behaviour limits the ac-

curacy over the interval of integration considered.

4.7 The matrix equation for the field strength

Choosing steps h^+ and h^- in regions L and R respectively, taking $\xi_0^{\mp} \neq 0$ and neglecting the noise, Eq.(4.1R) for the pivotal value $\xi^+ = \xi_i^+$, with $i = 0(1)$ N+1, is (See also section 4.3):

$$J_{tot}^+ = j\omega\varepsilon_o \, F(\xi_i^+) - \int_{\xi_i^+}^{\xi_{N+1}^+} F(\xi^+) \, k_1(\xi_i^+,\xi^+) \, d\xi^+ + \int_{\xi_o^+}^{\xi_i^+} F(\xi^+) \, k_{23}(\xi_i^+,\xi^+) \, d\xi^+ +$$

$$+ \int_{\xi_o^-}^{\xi_{N+1}^-} F(\xi^-) \, k_4(\xi_i^+,\xi^-) \, d\xi^- \qquad (4.22)$$

where $k_{23} = k_2 + k_3$, $\xi_{N+1}^+ = \xi_{c2}$ and $\xi_{N+1}^- = \xi_{c1}$. Approximating Eq.(4.22) by means of the trapezoidal rule, the following expression is found

$$J_{tot}^+ = j\omega\varepsilon_o \, F(\xi_i^+) +$$

$$- h^+ \left[\tfrac{1}{2} k_1(\xi_i^+,\xi_i^+) \, F(\xi_i^+) + k_1(\xi_i^+,\xi_{i+1}^+) \, F(\xi_{i+1}^+) + \ldots + \right.$$

$$\left. + k_1(\xi_i^+,\xi_N^+) \, F(\xi_N^+) + \tfrac{1}{2} k_1(\xi_i^+,\xi_{N+1}^+) \, F(\xi_{N+1}^+) \right] + \qquad i < N+1$$

$$+ h^+ \left[\tfrac{1}{2} k_{23}(\xi_i^+,\xi_o^+) \, F(\xi_o^+) + k_{23}(\xi_i^+,\xi_1^+) \, F(\xi_1^+) + \ldots + \right.$$

$$\left. + k_{23}(\xi_i^+,\xi_{i-1}^+) \, F(\xi_{i-1}^+) + \tfrac{1}{2} k_{23}(\xi_i^+,\xi_i^+) \, F(\xi_i^+) \right] + \qquad i > 0$$

$$+ h^- \left[\tfrac{1}{2} k_4(\xi_i^+,\xi_o^-) \, F(\xi_o^-) + k_4(\xi_i^+,\xi_1^-) \, F(\xi_1^-) + \ldots + \right.$$

$$\left. + k_4(\xi_i^+,\xi_N^-) \, F(\xi_N^-) + \tfrac{1}{2} k_4(\xi_i^+,\xi_{N+1}^-) \, F(\xi_{N+1}^-) \right] \qquad (4.23)$$

In matrix notation, the set of N+2 linear equations (4.23) can be written as

$$J^+_{tot} = (P^+ + j\omega\varepsilon_o I) F^+ + N^+ F^-$$

where $F^{\pm} = (F_o^{\pm}, F_1^{\pm}, \ldots, F_{N+1}^{\pm})^T$; $F_j^{\pm} = F(\xi_j^{\pm})$ with $j = 0(1)N+1$; $J^+_{tot} = (J^+_{tot}, \ldots, J^+_{tot})^T$; I is the identity matrix of the order N+2; P^+ and N^+ are square matrices of the order N+2. The elements of the matrices P^+ and N^+ can be calculated from Eq.(4.23).

Similarly, Eq.(4.1L) is replaced by a corresponding matrix equation

$$J^-_{tot} = (P^- + j\omega\varepsilon_o I) F^- + N^- F^+$$

The matrix equation for the whole inter-electrode space is

$$\begin{pmatrix} J^+_{tot} \\ J^-_{tot} \end{pmatrix} = \begin{pmatrix} M^+ & N^+ \\ N^- & M^- \end{pmatrix} \begin{pmatrix} F^+ \\ F^- \end{pmatrix} \tag{4.24}$$

where $M^+ = P^+ + j\omega\varepsilon_o I$ and $M^- = P^- + j\omega\varepsilon_o I$. Turning to a real matrix equation, Eq.(4.24) is equivalent to

$$J = H F \tag{4.25}$$

where

$$H = \begin{pmatrix} Re\ M^+ & Re\ N^+ & -Im\ M^+ & -Im\ N^+ \\ Re\ N^- & Re\ M^- & -Im\ N^- & -Im\ M^- \\ Im\ M^+ & Im\ N^+ & Re\ M^+ & Re\ N^+ \\ Im\ N^- & Im\ M^- & Re\ N^- & Re\ M^- \end{pmatrix}$$

$$J = \begin{pmatrix} \text{Re } J^+_{\text{tot}} \\ \text{Re } J^-_{\text{tot}} \\ \text{Im } J^+_{\text{tot}} \\ \text{Im } J^-_{\text{tot}} \end{pmatrix} \quad \text{and } F = \begin{pmatrix} \text{Re } F^+ \\ \text{Re } F^- \\ \text{Im } F^+ \\ \text{Im } F^- \end{pmatrix}$$

The matrices J and F are column vectors with $4(N+2)$ elements, the matrix H has order $4(N+2)$. Solving Eq.(4.25) would give us the required field strength F in the pivotal points. However, there is a snake in the grass.

In contrast with the functions k_1, k_2 and k_4, which are slowly varying functions in two variables, the function k_3 has a strongly oscillatory character when η_1 tends to zero. As a result, applying the trapezoidal rule to integrals, occurring in Eq.(4.22), such as

$$\int_{\xi_o^+}^{\xi_1^+} F(\xi^+) \, k_3(\xi_i^+, \xi^+) \, d\xi^+ \qquad (i \geq 0)$$

leads to terms in Eq.(4.25) that are too rough approximations of those integrals. Therefore, the following iterative procedure has been employed. In Eq.(4.25) replace $k_3(\xi_i^\pm, \xi_o^\pm)$ by zero, for $i \geq 0$ (Notice that $\xi_o^\pm$ is chosen approximately zero). Let $F^{(1)}$ be the solution of Eq.(4.25). Next, the left-hand member of that equation is replaced by a new one with the help of the solution $F^{(1)}$ obtained earlier. Illustrating this with the component $(\text{Re } J^+_{\text{tot}})_i$, the new component of J is given by the expression

$$(\text{Re } J^+_{\text{tot}})_i - \text{Re} \int_{\xi_o^+}^{\xi_1^+} F^{(1)}(\xi^+) \, k_3(\xi_i^+, \xi^+) \, d\xi^+ +$$

65

$$+ \text{Re} \left[\text{trapezoidal approximation, with two pivotal points,} \right.$$

$$\left. \text{of} \int_{\xi_o^+}^{\xi_1^+} F^{(1)}(\xi^+) \, k_3(\xi_i^+,\xi^+) \, d\xi^+ \right]$$

where $(J_{tot}^+)_i$ is equal to the enforced current density J_{tot}^+. Then, Eq. (4.25) with its new left-hand member is solved. Let its solution be $F^{(2)}$. By means of this solution Eq.(4.25) is again corrected, etc. When the sum of the absolute differences of the corresponding components of two successive solutions $F^{(n)}$ and $F^{(n+1)}$ (where n is a positive integer) is less than a prescribed number, the iteration is stopped. The final solution is a good approximation of the required h.f. electric-field strength $F(\xi_i^{\mp})$. The above technique is based on the fact that the integral of a function has a more quiet behaviour than the function itself.

Afterwards, the admittance Y per unit area can be computed by means of Eq.(3.35), where the integral in the denominator is calculated e.g. by applying Simpson's rule (This necessitates the choice of an odd number of pivotal points in region L as well as in region R).

Similarly, the noise temperature of the double-cathode tube can be computed along the rules given in Section 3.7. Here, too, the same matrix H plays a dominant part.

From now on, let Y be the actual admittance of the tube (the area of each of the cathodes is 7.94 mm^2). By subtracting from Y the admittance $j\omega C$ of the cold tube, we find the electronic admittance, i.e. the effect of the electrons alone.

The calculated real and imaginary parts of $Y - j\omega C$ have been plotted as a function of the d.c. voltage V in Fig. 4.5 for a typical set of parameters. The calculated noise temperature is plotted against the d.c. voltage V in Fig. 4.6. If $V = 0$, Nyquist's formula gives $T_n = T$. The cal-

66

culated value of T_n appears to be 1% higher than the assumed cathode temperature. In table 4.1 the numerical values of the calculated quantities are represented.
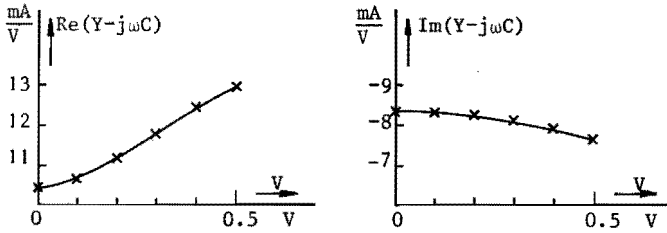

Fig. 4.5. Calculated real and imaginary parts of electronic admittance $Y - j\omega C$ vs. d.c. voltage V. Frequency 3 GHz, distance between cathodes 55 μm, temperature of cathodes 1300°K, saturation current density 3.537 A/cm^2, diameter of the cathodes 3.18 mm.
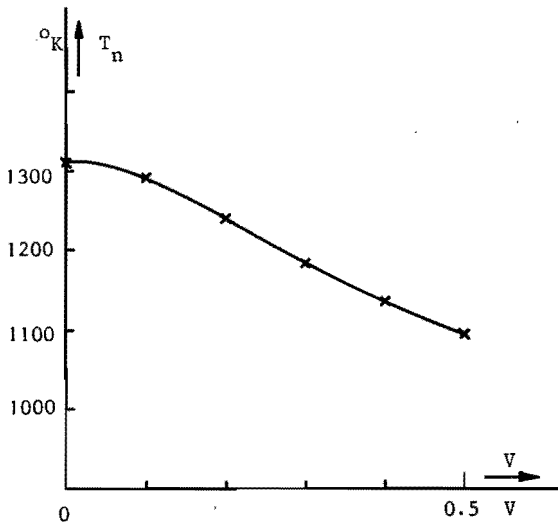

Fig. 4.6. Calculated noise temperature T_n of double-cathode tube vs. d.c. voltage V. Parameter values as in Fig. 4.5.

67

Table 4.1. Calculated admittances and noise temperatures (r = 1.59 mm) .

J_s [A/cm^2]	T [°K]	d [μm]	V [v]	Y - jωC [mA/v]	jωC [mA/v]	T_n [°K]
3.54	1300	55	0	10.4 - 8.36j	24.0	1310
			0.1	10.6 - 8.34j		1290
			0.2	11.1 - 8.28j		1240
			0.3	11.8 - 8.12j		1180
			0.4	12.4 - 7.90j		1130
			0.5	12.9 - 7.69j		1090
3.54	1300	45	0	17.9 - 13.5 j	29.3	1320
			0.5	20.9 - 10.7 j		1060
3.54	1300	20	0	116 - 50.6 j	66.0	1310
			0.2	114 - 44.5 j		1230
			0.5	107 - 30.5 j		1030
1.41	1300	55	0	9.32 - 8.33j	24.0	1310
			0.5	11.6 - 7.93j		1100
2.62	1400	50	0.2	14.5 - 10.7 j	26.4	1340
			0.5	16.4 - 9.49j		1170
1.46	1350	50	0	12.3 - 10.7 j	26.4	1370
			0.2	13.0 - 10.4 j		1290
			0.5	14.9 - 9.46j		1130

4.8 On the reliability of the numerical calculations

A number of checks on our computed results are available. The first one is founded on purely physical considerations. If we apply no voltage between the two cathodes of a double-cathode tube, thermodynamics predicts at any frequency a noise temperature T_n equal to the temperature of the

cathodes (Cf. section 2.3). Numerical calculations thus have to yield the predicted noise temperature. In all the cases that we computed, this is true within 2%, as can be seen from table 4.1. This check is a proof of the correctness of our computer program, but only for the case that both cathodes have the same d.c. potential.

For testing the program also for the case that there is a d.c. voltage between the cathodes, the following procedure turned out to be useful. Two independent ALGOL programs for the EL X 8 of the Department of Mathematics of the Eindhoven University of Technology were written by Van der Meijden[18] and the present author. Comparison of the results of the two programs, gave us an easy tool for detecting errors.

A different way of checking our program is to use it for computing the admittance and noise of normal diodes and comparing the results with those obtained by Löcherer[8]. For a particular set of parameter values Löcherer has computed the value $6.0 + 73.6j$ mS/cm^2 for the admittance Y per cm^2 (in his notation Y_{ges}) of a normal diode, and the value 0.26 for $F(\xi_{c2})$, where[*] $F(\xi_{c2})$ is the "Schwächungsfaktor des gesamten Kurzschluss-rauschstromes" of the diode. The parameter values for this case are given in Löcherer's expression (42), while the distance between cathode and anode is 175.6 microns. Using the same set of parameter values we have found the value $6.31 + 74.1j$ mS/cm^2 for the admittance Y per cm^2, and the value 1030°K for the noise temperature T_n, which corresponds with $F(\xi_{c2}) = 0.288$. The difference between the last number and the one obtained by Löcherer may be due to the fact that he has considered only 18 velocity classes of electrons, whereas we had 91. Löcherer has calculated his results partly manually, partly by means of a computer. His way of

---

[*] This should not be confused with the field strength $F(\xi^{\mp})$.

representing the computed values of Y in this case suggests an accuracy
lower than ours.

Hubert[9] has extended Löcherer's calculations very considerably. As a
check we also used one of Hubert's figures, viz. Fig. 14 ($j\omega\varepsilon_o$ $\underline{Y}$ in
Hubert's notation corresponds with our F). Since he does not give one of
his parameters as a number, this had to be read from the figure in ques-
tion. Our calculation yielded a curve for the solution $F(\xi^{\mp})$ of the equa-
tions (3.34L) and (3.34R) that coincides nearly with his. The relative
deviations are of the order of 2%.

Hence, we estimate to have a total relative error less than 2% for the
admittance Y as well as for the noise temperature T_n. The time needed by
the computer for calculating the admittance and the noise temperature was
1.5 hours for each set of parameters. Obtaining the potential distribution
and the transit angles took only about five minutes. These were, there-
fore, calculated with a much higher accuracy.

We can compare our computation of the potential distribution with the
results obtained by Lindsay et al.[2] They found, when $n_{c1}-n_{c2} = 0$:
$\xi^+ = 1.1498$ for $\eta = 0.75$ and $\xi^+ = 1.1825$ for $\eta = 0.80$. From this, linear
interpolation yields $\xi^+ = 1.1580$ for $\eta = 0.76256$. We have computed
$\xi^+ = 1.1582$ for $\eta = 0.76256$.

Finally, regarding the transit angle $\alpha^{\pm}$ of a normal diode, $\alpha^-(n_1,s) +$
$- \alpha^-(n_2,s)$ divided by $\omega A(m/2kT)^{\frac{1}{2}}$ (See section 4.2) has been computed for
$n_1 = 5$, $n_2 = 0.2$ and $s = -1$. We found 1.11694, while Paucksch[16] had
1.11692. Similarly, we computed $\alpha^+(n_1,s) - \alpha^+(n_2,s)$, divided by $\omega A(m/2kT)^{\frac{1}{2}}$,
resulting in 1.9878 for $n_1 = 3$, $n_2 = 0.4$ and $s = -1$. The corresponding
value calculated by Paucksch[16] is 1.98775.

5. RELATIVE IMPEDANCE OF THE TUBE MOUNTED IN A WAVEGUIDE

5.1 Introduction

So far the admittance and the noise of a double-cathode tube have been investigated in terms of voltages and currents. In this chapter the behaviour of such a tube when mounted in a waveguide will be investigated[19].

We mention the following related studies. Other authors have determined the admittance of a normal diode in a coaxial mount, as e.g. Hennings[20], or of a normal diode in a waveguide mount[21]. Vacuum tube diodes have been studied as microwave detectors at X-band by Dye et al.[22] and by Bronwell et al.[23]

A similar arrangement as in our double-cathode tube is often used for mounting semiconductor devices in a waveguide. Its theory was discussed e.g. by Van Iperen et al.[24]

5.2 Relative impedance of the tube. Transformation factor Q.

Fig. 5.1 shows the cross-section of a double-cathode tube. It can be placed between the broad sides of a waveguide (inner dimensions a and b; a > b). In principle it consists of two metal posts, the cathode-bearers, with a gap between them and surrounded by a coaxial glass wall. The extremities of the posts constitute the cathode surfaces. Between the posts an electron cloud is formed. By using a membrane it is possible to vary the distance between the cathodes d from 0 to 200 microns, which can be measured with a micrometer (not completely shown here).

Neglecting the glass wall, the tube can be considered as one cylindrical inductive obstacle consisting of two equal posts with a gap between them (Fig. 5.2), the posts being mounted symmetrically in a waveguide. In this approximation the electron cloud may be described by a
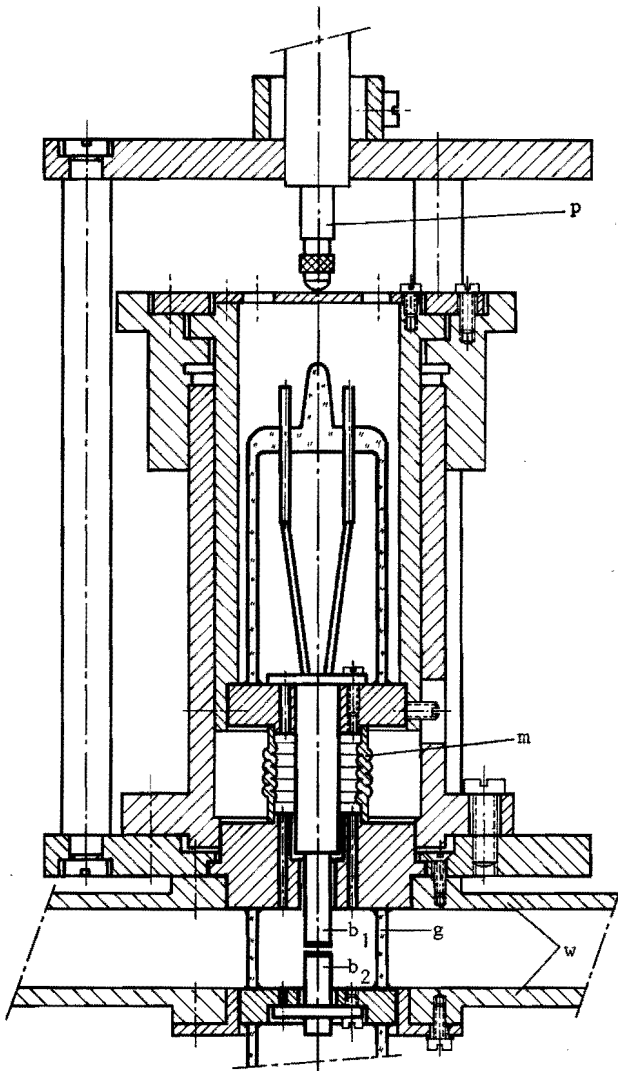
Fig. 5.1. Cross-section through double-cathode tube. The distance between the cathodes can be varied from 0 to 200 microns; b1, b2 = posts, at the ends of which are the cathode surfaces, g = glass wall, w = wall of waveguide, m = membrane, p = part of micrometer.
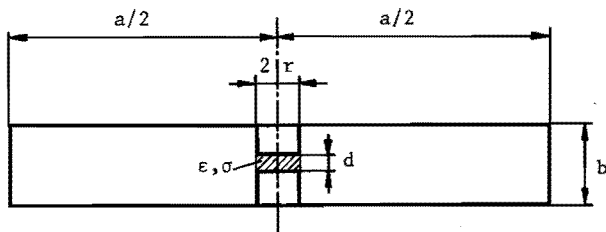
72

Fig. 5.2. Cross-section through waveguide with cylindrical obstacle. The gap is filled with a medium with dielectric constant ε and specific conductance σ.

medium with a dielectric constant ε and a specific conductance σ. It is further assumed that the walls of the waveguide and the posts have an infinitely high conductance. The equivalent T-network of such an obstacle is shown in Fig. 5.3. Let both the input reference plane 1 and the output reference plane 2 coincide with the plane of the post. Assuming $r \ll \lambda_o$ (where r is the radius of the post and λ_o is the wavelength in vacuum), $|z_{11}-z_{12}|$ and $|z_{22}-z_{12}|$ are very small, so that the obstacle may be represented by a single relative impedance z_{12}.
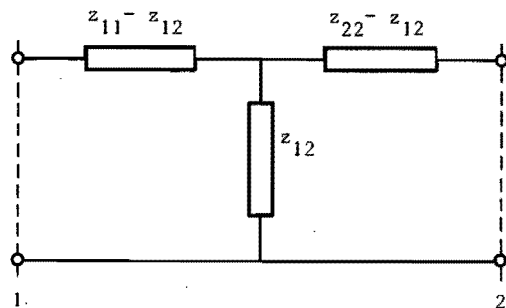

Fig. 5.3. Equivalent T-network of obstacle with gap. It is characterised by the relative impedances z_{11}, z_{22} and z_{12}.

73

Now consider z_{12} as a series connection of $z_{12}^{(o)}$ (the impedance of the obstacle without the gap) and an additional impedance representing the action of the gap

$$z_{12} = z_{12}^{(o)} + z_{gap} \qquad (5.1)$$

with

$$z_{gap} = Z/Z_o Q \qquad (5.2)$$

Here $Z = 1/Y = 1/(G + jB)$; $G = \sigma\pi r^2/d$; $B = \omega\epsilon\pi r^2/d$; Z_o is the characteristic impedance of the waveguide defined as $Z_o = (\mu_o/\epsilon_o)^{\frac{1}{2}} (\lambda_g/\lambda_o)$; λ_g is the wavelength in the guide, and Q is a transformation factor. If $d \ll b$, then

$$Q = \frac{2b}{a} \left\{ 1 + \frac{4d}{\epsilon_r br} F \right\} \qquad (5.3)$$

with

$$F = \sum_{m=1}^{\infty} \frac{K_1(k_m r)}{k_m K_o(k_m r)} \left\{ \frac{\sin(m\pi d/b)}{m\pi d/b} \right\}^2$$

and

$$k_m = \left\{ \left(\frac{2m\pi}{b} \right)^2 - \left(\frac{2\pi}{\lambda_o} \right)^2 \right\}^{\frac{1}{2}}$$

where K_n is the modified Bessel function of the second kind and order n, and $\epsilon_r = \epsilon'/\epsilon_o$, the complex dielectric constant ϵ' being defined by

$$\epsilon' = \epsilon - \frac{j\sigma}{\omega}$$

An expression for $z_{12}^{(o)}$ can be found in Kato et al.[21] It turns out that for our configuration the dominant term in (5.3) is $2b/a$, i.e. more

than 80% of the absolute value of Q for all cases that occurred.

In principle, in the case of a vacuum gap (ε_r = 1) the theory has been given by Kato et al. It could be applied, with minor alterations, to explain experiments we performed on such obstacles[25].

Heijnemans[26] has generalised the results of Kato and Isobe for the case that the relative dielectric constant ε_r is not equal to one. In particular, he has derived Eq.(5.3).

We have treated the numerical calculation of the transformation factor Q elsewhere[25], when ε_r = 1 (Remember that here an extra factor 2 is incorporated in the definition of Q).

5.3 Measurements of relative impedances

5.3.1 Measuring method

The impedance measurements were carried out at a frequency of 3.03 GHz. The measuring set-up is shown in Fig. 5.4. We used the method of
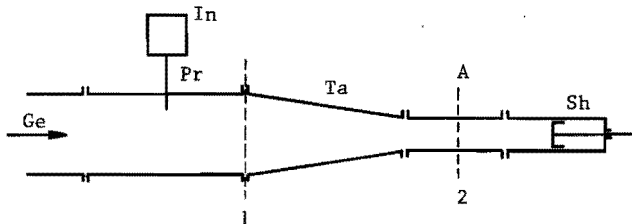

Fig. 5.4. Measuring arrangement; Ge = generator, Pr = probe, In = indicator, Ta = taper, A = position of tube, Sh = movable short-circuit, 1,2 = reference planes.

Deschamps[27,28] in a somewhat modified form. The frequency of the generator, a reflex klystron, was stabilised by phase-locking it to a 1 MHz

75

quartz crystal oscillator (the long term stability of the crystal oscilla-
tor is $5:10^8$ per week).

The standing wave measurements (Cf. Fig. 5.4) were carried out with a
very accurate slotted line (inner dimensions of the waveguide 72 × 34 mm).
The tubes we used were placed in a waveguide with inner dimensions
72 × 10 mm. The linear taper was about 370 mm in length.

By means of the method of Deschamps the scattering matrix S of the
tube can be calculated. From S the impedance matrix Z can be derived:

$$Z = (I + S)(I - S)^{-1}$$

with

$$Z = \begin{pmatrix} z_{11} & z_{12} \\ z_{12} & z_{22} \end{pmatrix}$$

I is the identity matrix of order 2 and $(I - S)^{-1}$ is the inverse matrix
of I − S. Of course, the reference planes in Fig. 5.4 are not the ref-
erence planes in respect of which the impedance matrix Z is calculated
(See section 5.2).

Since the measuring method was described elsewhere[25,29], we refer the
reader to these papers for further details. In this connection we only ob-
serve that a linear taper always causes reflections near its ends[30], and
that the concept of the least-square circle[29] is very useful for numer-
ical data processing of reflection coefficient circles (Cf.[31]).

Finally, we would mention that the measurements themselves can be
performed with an accuracy better than 2% using the above method.

5.3.2 Measurements on cold tubes and their discussion

When the heater supplies are switched off, the double-cathode tube

76

behaves as an inductive post with a capacitive gap. As a first example, experimental results measured on tube No. 1 are shown in Fig. 5.5.
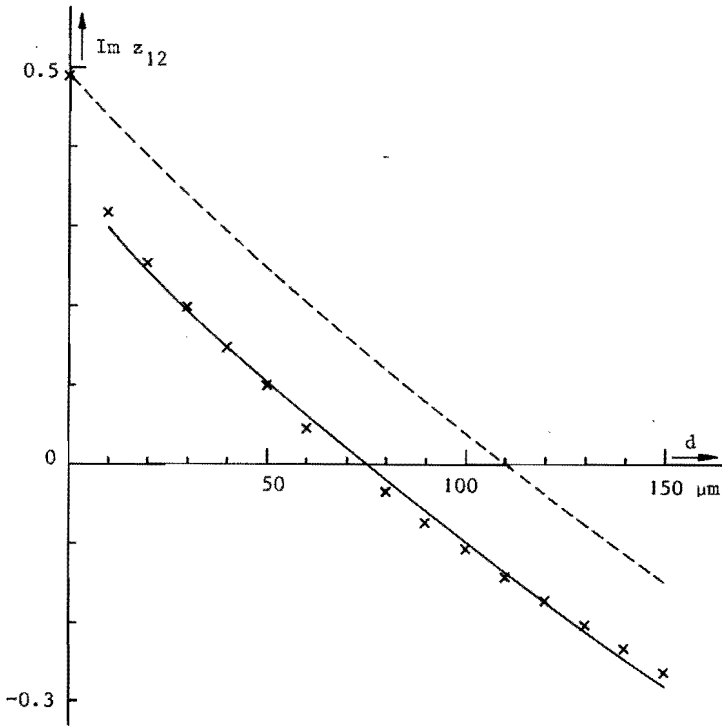

Fig. 5.5. Im z_{12} vs. distance d for cold tube No. 1. Parameter values are: frequency 3.03 GHz, diameter of cathodes 3.18 mm, inner dimensions of waveguide 10 x 72 mm. The solid line is the theoretical curve with skewness $\delta = 78$ μm and effective radius $r_{eff} = 1.55$ mm, best fitting the experimental points. The dotted line represents the theoretical curve with $\delta = 0$ and $r_{eff} = 1.55$ mm.

Neglecting the glass wall the theoretical curve for the cold tube can be calculated (section 5.2), if the extremities of the cathode bearers

77

are parallel. A refinement of the theory was set up[25] for the case that

the gap-width varies linearly from d to d + δ. The effective distance

d_{eff} is then given by the following expression

$$d_{eff} = \frac{1}{2}\left\{ d + \frac{\delta}{2} + \left(d\delta + d^2 \right)^{\frac{1}{2}} \right\}$$
(5.4)

Since the axes of the cathode bearers do not coincide with each other,

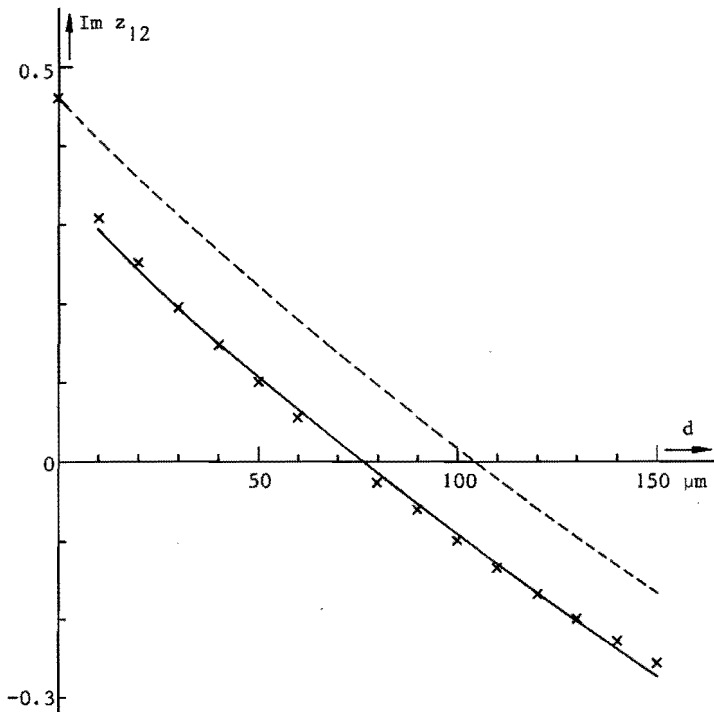the l.f. capacitance C occurring between the bearers will be less than

Fig. 5.6. Im z_{12} vs. distance d for cold tube No. 2. The skewness is

δ = 64 microns. The effective radius is 1.57 mm. See further the caption

of Fig. 5.5.

may be expected according to the actual radius r. In order to bring this into account, an effective radius r_{eff} is introduced so that by definition $C = \epsilon_o \pi r_{eff}^2/d_{eff}$. Comparing the experiments with the theory (Cf. Fig. 8 of reference[25]) and using the method of least squares adapted for non-linear equations, the values of the skewness δ and the effective radius r_{eff} are found. For tube No. 1 the skewness δ is 78 microns and r_{eff} is 1.55 mm. The former corresponds with an angle of 1.4 degrees between the two cathode surfaces. With the help of the above values for δ and r_{eff} the curve of Im z_{12} vs. the distance d has been calculated (Fig. 5.5: solid line).

The determination of δ depends strongly on one measurement, viz. that of $z_{12}^{(o)}$. We estimate the accuracy with which d_{eff} is determined to be 3 microns.

In Fig. 5.6 similar results are represented for tube No. 2. Here the skewness and the effective radius are 64 microns and 1.57 mm, respectively.

5.3.3 Measurements on hot tubes

When determining impedance and noise (see chapter 6), the two cathodes should have the same temperature. However, the temperature of one of the cathodes was adjusted slightly in order to get a d.c. current $I = 0$ when the applied d.c. voltage $V = 0$. The resulting difference in temperature was at most $10^\circ K$.

From the experimental data the relative impedances z_{12} and z_{gap} (Eq. (5.1)) have been calculated. The value of $z_{12}^{(o)}$ was determined by measurements on the cold tube. In Figs. 5.7 and 5.8 the relative impedances z_{gap} are plotted as functions of the applied d.c. voltage V for tubes No. 1 and No. 2, respectively.

Re z_{gap}
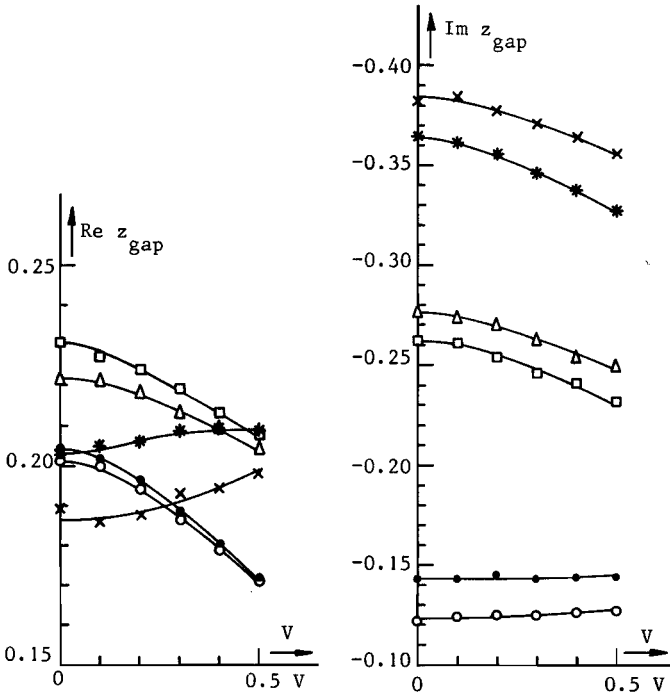
0.25

0.20

0.15

0   0.5 V

V

Im z_{gap}

-0.40

-0.35

-0.30

-0.25

-0.20

-0.15

-0.10

0   0.5 V

V

Fig. 5.7. Experimental values of real and imaginary parts of z_{gap} vs. d.c. voltage V for tube No. 1. Frequency 3.03 GHz.

Distances d between cathodes: 20 μm, 30 μm, 40 μm

cathode temperature 1300°K   ●   Δ   ✗

cathode temperature 1350°K   ○   □   ✳

5.4 Discussion of the results

5.4.1 The parameters of the measurements

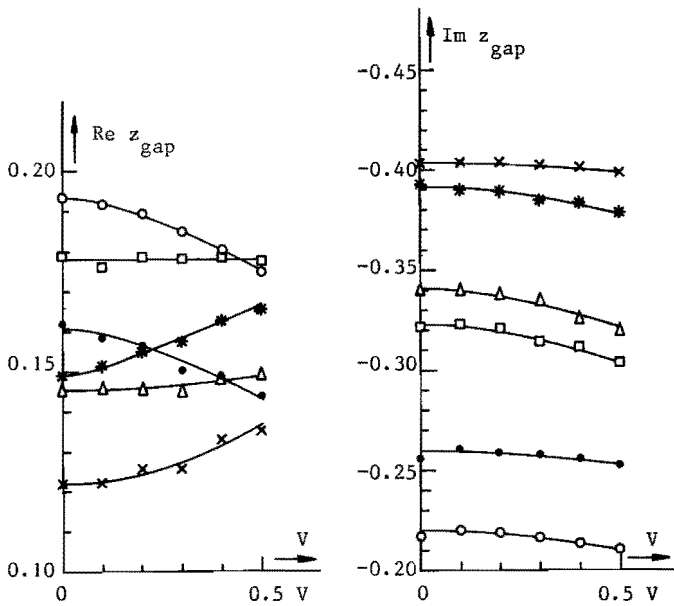In order to be able to compare the theory with the experimental data,

Fig. 5.8. Experimental values of the real and imaginary parts of z_{gap} vs. d.c. voltage V for tube No. 2. The parameter values are the same as in Fig. 5.7.

we have to know the values of the following parameters during the measurements:

(a) the frequency

(b) the effective radius of the cathodes

(c) the distance between the cathodes

(d) the temperature T of the cathode surfaces

(e) the saturation current density J_s

(f) the d.c. voltage V applied between the cathodes

(g) the inner dimensions of the waveguide.

The effective radius is found from the measurements on the cold tube, while the distance d is determined by means of a micrometer and has after-

wards to be corrected for skewness (See section 5.3.2). Eq.(5.4) for the

effective distance is valid when the admittance Y is inversely propor-

tional to the distance. However, from the data of table 4.1 it can be

found that the real and imaginary parts of the admittance Y vary accord-

ing to d^a, where $-1 < a < -2$. Using a similar method as in reference[25],

we derived a formula for d_{eff} if Y varies with d^{-2}. This yielded values

of d_{eff} that deviated from those calculated by means of Eq.(5.4) by at

most 3 microns in the cases we investigated experimentally. Therefore, we

used Eq.(5.4) in all our calculations.

The temperature T was found pyrometrically. The true temperature of

the cathodes is obtained by applying a correction of 80°K. Herewith the

absorption of the glass wall and the emission coefficient of a tungsten

cathode surface[32] have been taken into account.

The saturation current density was determined in the following way.

Switching off one of the heaters and using pulse techniques, the normal

diode characteristic was made visible on an oscilloscope. From such char-

acteristics the saturation currents of the cathodes were easily found

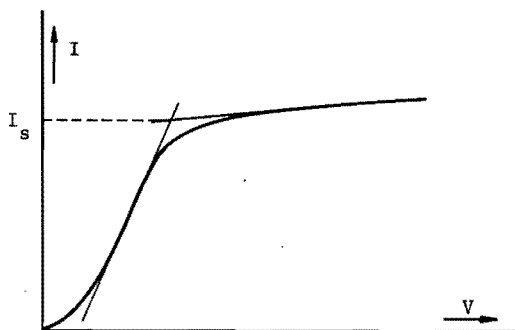(Fig. 5.9). The saturation currents of the two cathodes of one tube may

Fig. 5.9. (I,V) characteristic of a normal plane diode. The point of in-

tersection of the tangents determines the saturation current I_s.

differ as much as 30%. Nevertheless, in order to simplify the numerical calculations, we assumed that both cathodes had the same saturation current, viz. the mean of the values found. This is justified by the fact that the value of the saturation current does not affect the results very much (see table 4.1).

The manner in which the other parameters are determined is self-evident.

5.4.2 Comparison of experiments with theory

In order to compare the experimental values with our theoretical calculations, we need a relation between the relative impedance z_{gap} and the electronic admittance $Y-j\omega C$. It can be derived from Eqs.(5.2) and (5.3):

$$Y - j\omega C = - j\omega C \left(1 + \frac{4d}{br} F \right) + \frac{a}{2bZ_o} \frac{1}{z_{gap}} \tag{5.5}$$

where $C = \varepsilon_o \pi r^2/d$ is the l.f. capacitance of the gap for vacuum. By means of Eq.(5.5) the experimental values of the electronic admittance $Y-j\omega C$ have been determined for both tubes from the data given in Figs. 5.7 and 5.8. The results are shown in Figs. 5.10, 5.11, 5.12 and 5.13 together with the theoretical ones (see table 4.1).

Observe that in applying Eq.(5.5), it is necessary to use for d in that formula the value of d_{eff} calculated by means of Eq.(5.4), and for r the value of r_{eff}.

Comparing the experimental and theoretical data for both tubes, the deviations can be explained by the expected measuring errors of d_{eff}, except for $Re(Y-j\omega C)$ of tube No. 1 (Fig. 5.10), where the deviation is 10μm.

83

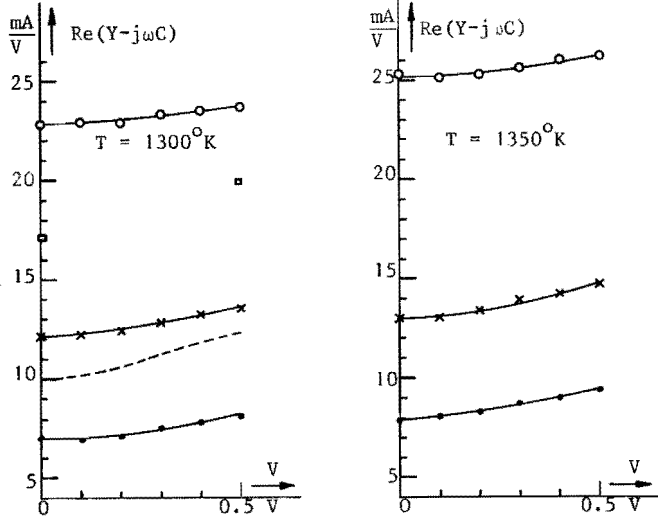Fig. 5.10. Real part of Y-jωC vs. d.c. voltage V for tube No. 1. Skewness δ = 78 μm, effective radius = 1.55 mm.

Experimental: f = 3.03 GHz, d_{eff} = 51 μm (o), 62 μm (×), and 73 μm (●).

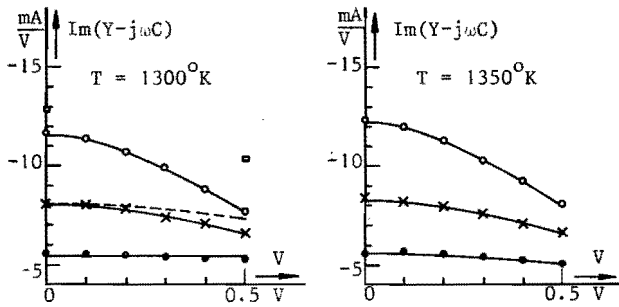Theoretical: f = 3 GHz, J_s = 3.54 A/cm^2; d = 55 μm (dotted line),

d = 45 μm (□).

Fig. 5.11. Imaginary part of Y-jωC vs. d.c. voltage V for tube No. 1. For further data see caption of Fig. 5.10.
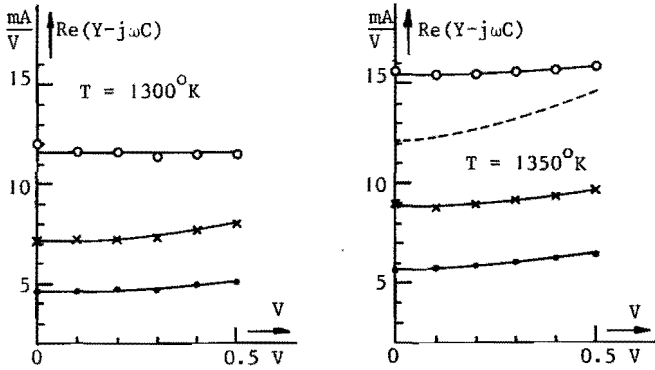
Fig. 5.12. Real part of Y-jωC vs. d.c. voltage V for tube No. 2. Skewness δ = 64 μm, effective radius = 1.57 mm.

Experimental: f = 3.03 GHz, d_{eff} = 46 μm(o), 57 μm(×), and 67 μm(•).

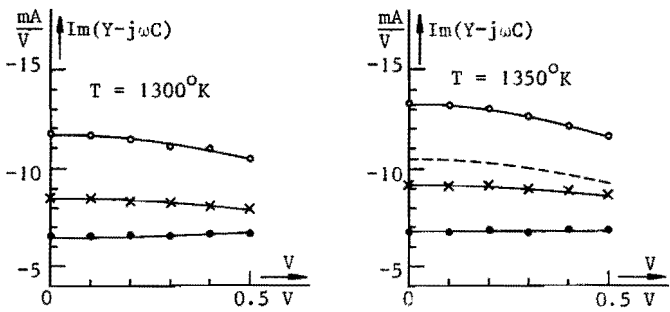Theoretical (dotted line): f = 3 GHz, d = 50 μm, J_s = 1.46 A/cm^2.

Fig. 5.13. Imaginary part of Y-jωC vs. d.c. voltage V for tube No. 2. For further data see caption of Fig. 5.12.

85

So far we have neglected the influence of the glass wall on the meas-
uring results. This we were permitted to do, because it has been largely
taken into account by subtracting from z_{12} the measured value of $z_{12}^{(o)}$
(see section 5.3.3), which is also affected by the presence of the glass
wall. However, the glass wall had yet another effect on the measurements.
When the cathodes of the tube were at a high temperature, metal parts of
the cathodes precipitated on the glass wall. This caused the properties of
the tube to vary slowly during the measurements. Although, obviously, its
influence on $z_{12}-z_{12}^{(o)}$ is not so large, part of the discrepancy may be due
to this phenomenon. Its effect on noise is more pronounced. In chapter 6
we shall return to this subject.

5.4.3 Comparison of l.f. with h.f. admittance

    If there is no potential difference between the two cathodes, the l.f.
admittance g of the tube is given by the following expression (see Eq.
(1.5))

$$g = \frac{q}{kT} \, I_s \, \exp(-\eta_{c1})$$

where I_s is the saturation current of each of the cathodes. For
$J_s = 3.54 \text{ A/cm}^2$, $T = 1300^\circ\text{K}$, and $V = 0$ the theoretical values of g and
Re Y are represented in table 5.1. Since with increasing distance the po-

Table 5.1. Values of g and Re Y when V = 0

d [μm]	g [mA/V]	Re Y [mA/V]
20	138	116
45	32.9	17.9
55	22.8	10.4

tential minimum becomes deeper, the l.f. and h.f. values of the electronic

conductance decrease. If the distance is 20 microns, the transit time ef-

fects are not yet very important so that the difference between the two

values is small. For larger distances the h.f. values of the electronic

conductance is decreasing more rapidly as transit times become larger.

As regards the influence of the saturation current, we find, compar-

ing the theoretical results (table 4.1) for a large change of J_s, viz.,

from 3.54 A/cm^2 to 1.41 A/cm^2 (with T = 1300°K and d = 55 µm) that Re Y

changes about 10% and that Im Y is practically constant. It is conceivable

that the influence is so small, because the density of the d.c. electron

current j flowing from one cathode to the other is almost independent of

the saturation current density. From Eq.(1.5) and the value of g given in

table 5.1 it can be calculated that j = 32.1 mA/cm^2 if J_s = 3.54 A/cm^2

(and V = 0), while we found j = 29.7 mA/cm^2 if J_s = 1.41 A/cm^2, so that

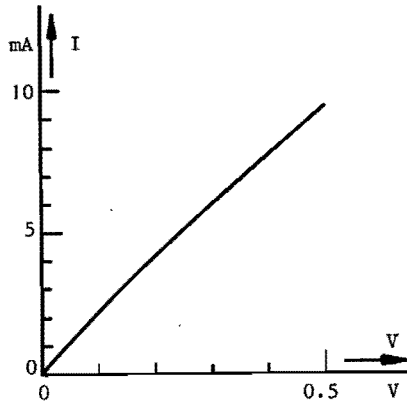the change of j, and hence also of g (Eq.(1.5)), is only 8%.

Fig. 5.14. Theoretical (I,V) characteristic of a double-cathode tube. For
the other parameters see caption of Fig. 4.5.

The calculations treated in chapter 4 provide also the (I,V) characteristic of a double-cathode tube, which is shown in Fig. 5.14. It appears from it that g decreases with increasing V. At high frequencies the behaviour of the electronic admittance Re Y as a function of V depends on the distance d. If d = 20 μm, Re Y also decreases with increasing voltage. As has already been stated, at that distance the influence of the transit times is small and then we may expect that the behaviour of Re Y is similar to that of the l.f. admittance g. If d = 50 μm, however, the influence
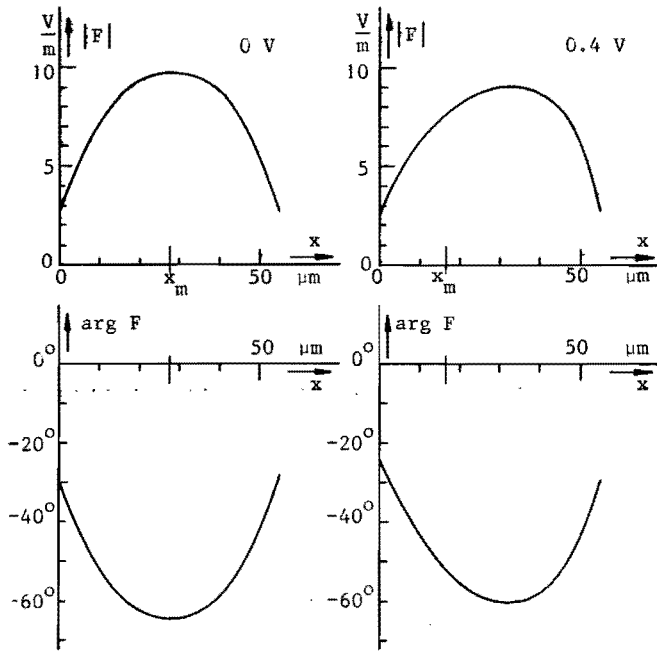

Fig. 5.15. Theoretical curves for the complex amplitudes of the h.f. field-strength distributions (absolute values and arguments). Applied d.c. voltages are zero (left) and 0.4 volt (right). Amplitude of a.c. total current density 1 A/m^2. For the other parameters see caption of Fig. 4.5.

of the transit times is large. They decrease with increasing d.c. voltage, and consequently, the real part of Y as well as its imaginary part must increase, as is indeed shown in Figs. 5.10 to 5.13 inclusive.

5.4.4 Space-charge waves in a double-cathode tube

Our computer programs give also information on the a.c. field in the space between the cathodes. From a physical point of view it is interesting to consider the absolute values and the phases of (a) this field, (b) its integral, the a.c. potential, and (c) its derivative, as functions of x . The derivative represents the a.c. part of the space-charge density.
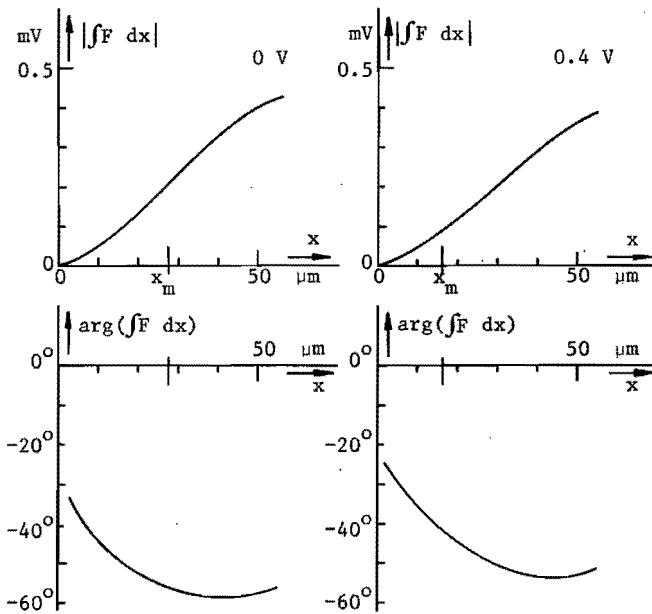

Fig. 5.16. The complex amplitudes of the a.c. potentials plotted vs. x (absolute values and arguments). For the parameters see caption of Fig. 5.15.

89

The h.f. field-strength distributions are shown in Fig. 5.15 for two typical sets of parameters. As can be seen on the right of the figure, the field strength F at cathode c_1 is nearly equal to that at cathode c_2. This is to be expected, because the stationary space-charge densities at the two cathodes are equal within 0.5% (Eq.(2.10)).

In Fig. 5.16 are plotted the absolute values and the arguments of the a.c. potentials for the same parameter values. It turns out that the amplitudes of the a.c. potentials grow more or less linearly.

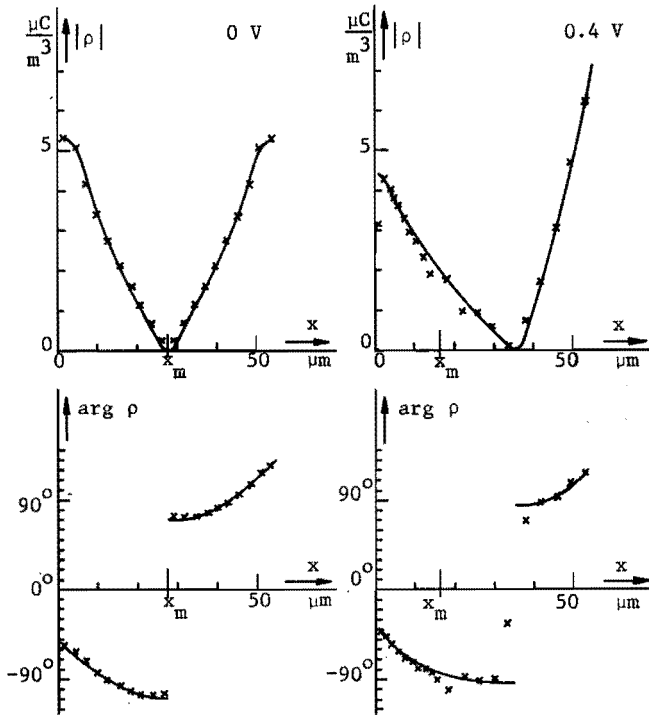The most interesting results are found by considering the derivative

Fig. 5.17. The complex amplitudes of the a.c. parts of the space-charge densities ρ vs. x (absolute values and arguments). For the parameters see caption of Fig. 5.15.

of F, which is proportional to the a.c. space-charge density ρ (Fig. 5.17). There appears to be a point where its amplitude is zero. If no voltage is applied, this point coincides with the potential minimum. Hence, although an a.c. current is flowing through the tube, the space-charge density in the potential minimum remains constant. Looking also at arg ρ as a function of x, we see that a space-charge wave is travelling from cathode c_1 towards the potential minimum with decreasing amplitude and increasing phase velocity, which seems to be infinite when the wave reaches the potential minimum. The phase of -50° at cathode c_1 means that a maximum of the electron density is leaving this cathode 50/360 of a period after the current from c_2 to c_1 has reached its maximum value. A space-charge wave also starts from cathode c_2. This wave is in opposite phase with the wave starting from c_1. The two waves arrive at the potential minimum with a phase difference of 180° and thus would annihilate each other if their amplitudes had not already become zero.
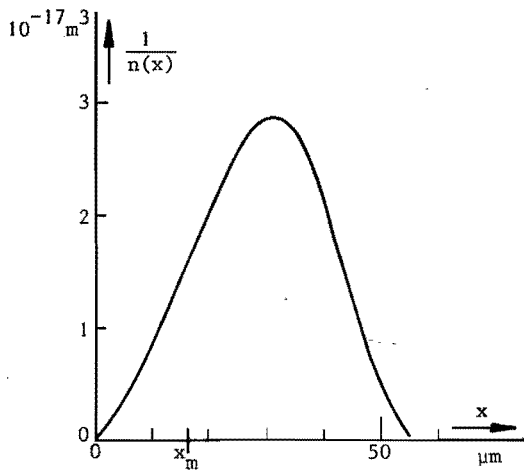

Fig. 5.18. The inverse of the volume density n(x) of the electrons plotted against x, if the applied d.c. voltage is 0.4 volt. For the other parameters see caption of Fig. 4.5.

When a d.c. voltage of 0.4 volt is applied, there are likewise two
space-charge waves starting from the two cathodes. The point where they
meet now with zero amplitudes and a phase difference of 180° is not the
potential minimum. It lies nearest to the cathode with the highest poten-
tial, while the potential minimum lies nearest to the other cathode. The
former point seems to coincide with the point of minimum d.c. space-charge
density. In order to show this, the inverse of the volume density $n(x)$ of
the electrons, calculated with the aid of Eq.(2.10), is represented in
Fig. 5.18. As regards the phase difference between space-charge waves and
current, the situation is roughly the same as in the case of no voltage.
The space-charge waves are now starting from the cathodes in almost oppo-
site phases. Their phase differences with the current are about -40° and
-60°, respectively.

6. NOISE TEMPERATURE OF THE TUBE

6.1 Introduction

In order to measure its noise temperature T_n, the double-cathode tube has to be matched to the waveguide. We have found that this is more easily done in a waveguide with reduced height. In our case we obtain a VSWR less than 1.2 over a band width of 70 MHz around the centre frequency of 3 GHz. The frequency of the i.f. amplifier of our Dicke radiometer[33] is 30 MHz.

6.2 Matching of the tube to the waveguide

The tube is mounted in a waveguide with a movable short-circuit, which comes nearly $\lambda_g/4$ after the tube, and with an adjustable probe near the tube (Fig. 6.1). The latter is matched to the waveguide by adjusting the depth of the probe, the distance d between the cathodes, and the position of the short-circuit Sh, when the applied d.c. voltage equals zero. Keeping d fixed, matching is obtained for other voltages by slightly adjusting the plunger and the probe.

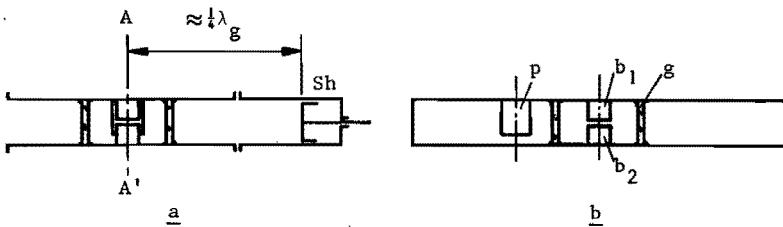
Fig. 6.1. Tube mounted in waveguide with adjustable probe p and movable plunger Sh, situated nearly $\frac{1}{4}\lambda_g$ after the tube (left). Cross-section AA' (right); g = glass wall, b_1, b_2 = posts, at the ends of which are the cathode surfaces (Cf. Fig. 5.1).

93

In Fig. 6.2 the set-up is given with which the matching of the tube
to the waveguide is carried out. The source B supplies a signal the fre-
quency of which is swept linearly with time. Entering the waveguide via
the adapter Ad_2, the signal is split into two parts by the directional
coupler C. The first part is detected by the crystal detector D_2. The de-
tected signal is used for the automatic level control ALC of source B.
The other part of the signal enters the measuring arm. If reflection oc-
curs at the taper Ta and the load A, which is the waveguide circuit shown
in Fig. 6.1, the reflected wave can be made visible with the help of the
detector D_1 and the oscilloscope Osc. When the frequency characteristics
of the two ways are equal, one can obtain quickly an insight into how well
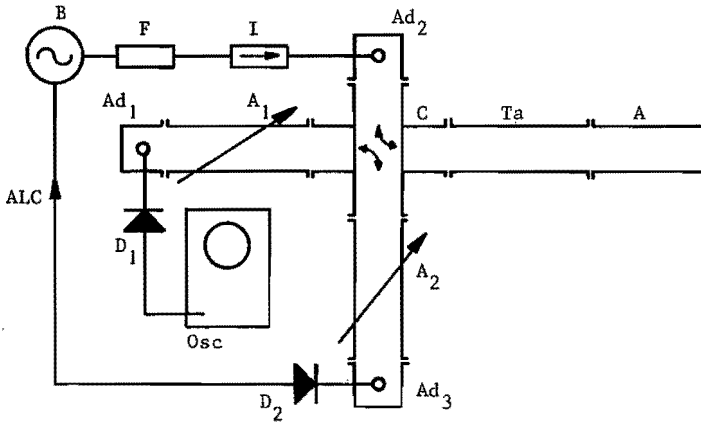the tube is matched.

Fig. 6.2. Set-up for matching the tube to the waveguide. B = signal
source, F = bandpass filter, I = isolator, Ad_1, Ad_2, Ad_3 = coaxial-to-
waveguide adapters, A_1, A_2 = attenuators, D_1, D_2 = detectors, Ta = taper,
A = load, Osc = oscilloscope, ALC = automatic level control, C = direc-
tional coupler.

Finally, the matching has to be checked by point-to-point measurements with the help of a slotted line that is placed between the directional coupler C and the taper Ta.

6.3 Noise temperature measurements

6.3.1 Measuring methods

The arrangement for the noise measurements is shown in Fig. 6.3. It
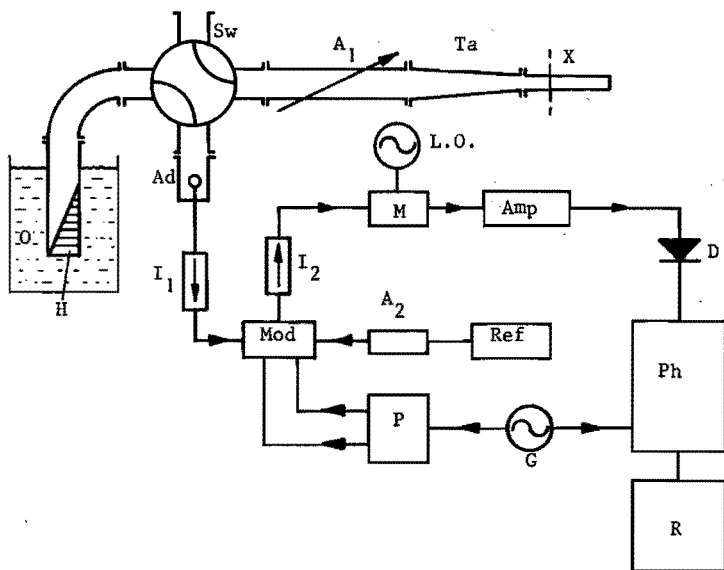
Fig. 6.3. Set-up for noise temperature measurements. O = oil bath, H = hot load, Sw = waveguide switch, A_1 = precision attenuator, Ta = taper, X = matched noise source with unknown noise temperature, Ad = coaxial-to-waveguide adapter, I_1, I_2 = isolators, Mod = PIN modulator, A_2 = attenuator, Ref = reference noise source, M = balanced mixer, L.O. = local oscillator (3 GHz), Amp = i.f. amplifier, D = detector, Ph = phase sensitive amplifier, G = l.f. generator (1 kHz), P = pulse former, R = recorder.

is a variant of the well-known Dicke radiometer (Cf.[33]). It contains

three noise sources, viz. the standard noise source H that is placed in a

temperature-controlled oil bath O, the reference noise source Ref and the

noise source X, of which the noise temperature has to be measured. Here X

is the double-cathode tube.

Let us first assume that the switch Sw is in the position shown in

Fig. 6.3. The PIN modulator switches alternatingly (with a frequency of 1

kHz) the noise from the hot load H and the noise from the noise source

Ref. After the signal is mixed with the local oscillator signal, the fre-

quency of which is about 3 GHz, in the balanced mixer M, the resultant

signal is fed into the i.f. amplifier Amp (with centre frequency 30 MHz).

The signal obtained is detected. It is then amplified by means of a phase

sensitive amplifier Ph and supplied to a recorder R. With the attenuator

A_2 the noise signal from the source Ref can be adjusted in order to get

zero output at the recorder R (zero method). Then the Dicke radiometer

has the highest sensitivity. Switching the waveguide switch Sw, the pre-

cision attenuator A_1 is adjusted in such a way that the noise from the

matched load X causes a signal output v_1 on the recorder R just above

zero. Next, the attenuator A_1 is adjusted to obtain an output signal v_2

just below zero. Linear interpolation between v_1 and v_2 yields the value

of the attenuation a of the attenuator A_1 needed for equilibrium between

the two positions of switch Sw (substitution method).

The noise temperature T_X of source X is then given by the following

expression

$$T_H = a \, T_X + (1-a) \, T_o \tag{6.1}$$

where T_H = absolute temperature of the hot load H, T_o = absolute tempera-

ture of A_1 = room temperature.

It is not necessary to know the noise temperature of the reference source Ref. It can be a 10PM noise diode[34] or a gas-discharge tube[35].

We observe that in reality we combined the measuring equipments, which are sketched in Figs. 6.2 and 6.3 in order to be able to check the matching of load X with taper while determining the noise temperature.

The above method presents the difficulty that the value of $T_H - T_o$ has to be known accurately, since $T_H \ll T_X$. A better though more time-consuming method is the following. Instead of a hot load in an oil bath, a hot load H in a furnace is used. Part of the measuring arrangement in this case is shown in Fig. 6.4. The temperature of the noise standard H can easily be 1200 or 1300°K. For rapid adjustment of the equilibrium in noise temperature between the two positions of the waveguide switch, the
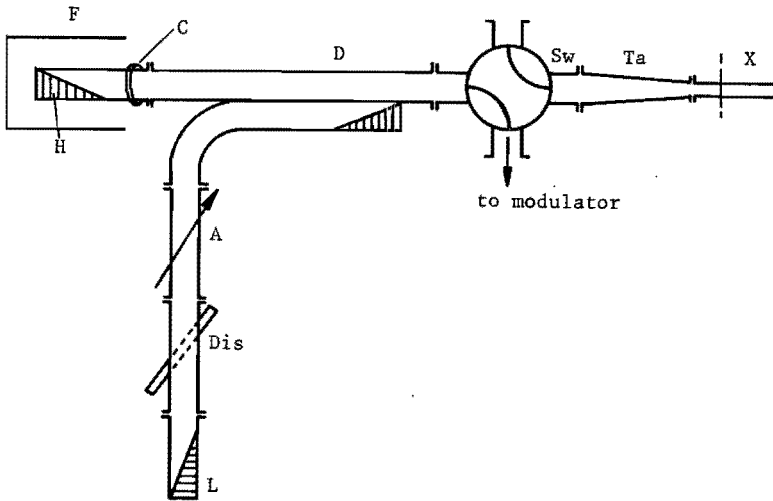

Fig. 6.4. Part of measuring arrangement with hot load H in furnace F. Dis = gas-discharge tube (K51A); A = precision attenuator, L = matched load, D = directional coupler (20 dB), C = water cooling. See further Fig. 6.3.

temperature T_H of the load H is chosen just below the unknown noise temperature T_X. The difference is compensated for by noise, originating from a gas-discharge tube. If there is equilibrium, the following expression is valid

$$T_X = (1-b) T_H + b\left\{a T + (1-a) T_o\right\}$$ (6.2)

where T = noise temperature of the gas-discharge tube, a = attenuation factor of the attenuator A, b = coupling factor of the directional coupler, and T_o = absolute temperature of the attenuator A.

6.3.2 Measurements on double-cathode tubes

Using a standard noise source in an oil bath (Fig. 6.3), the noise temperature of tube No. 1 has been measured as a function of the applied d.c. voltage V (Fig. 6.5). The theoretical curve has been computed for a
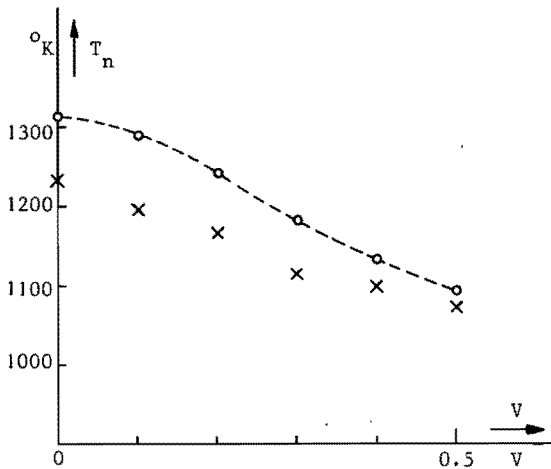

Fig. 6.5. Noise temperature T_n of tube No. 1 vs. d.c. voltage V. Parameter values for the theoretical curve (dotted line) as in Fig. 4.5. Crosses indicate the experimental points, with: frequency of local oscillator 2.98 GHz, distance between the cathodes 30 μm, skewness 78 μm, temperature of cathodes 1300°K.

98

distance of 55 microns between the cathodes and a frequency of 3 GHz (See also table 4.1). Each experimental point is the average of three measurements.

The results for tube No. 2 have been obtained in a similar manner. The experimental points are shown in Fig. 6.6, each of which is the average of two measurements. The noise temperature T_n has been calculated only for V = 0.2 and 0.5 volt, respectively. According to Nyquist T_n is known for V = 0. This yields a third point for the theoretical curve in Fig. 6.6.

Observations on other tubes can be found in table 6.1. In these cases the noise temperature has been measured only for equal potentials of the two cathodes. The second column of table 6.1 shows the frequency, which

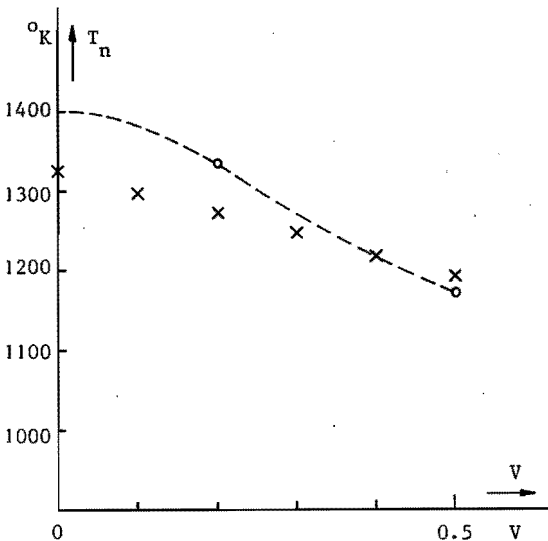Fig. 6.6. Noise temperature T_n of tube No. 2 vs. d.c. voltage V. Theoretical (dotted line): J_s = 2.62 A/cm^2, T = 1400°K, d = 50 μm, f = 3 GHz. Experimental: T = 1400°K, d = 30 μm, δ = 64 μm, frequency of local oscillator = 2.98 GHz.

Table 6.1

tube No.	freq. [GHz]	band width $S \leq 1.2$	temp. of cathodes pyrometric [°C]	true [°K]	T_n [°K]	average of T_n [°K]	noise source
3	3.00	75MHz	1050	1400	1381	1379	hot load in oil
					1400		
					1356		
					1379		
					1363	1359	hot load in furnace
					1357		
					1354		
					1366		
					1352		
4	2.98	70MHz	950	1300	1230	1219	hot load in furnace
					1217		
					1218		
					1221		
					1223		
					1217		
			1000	1350	1275		
			1050	1400	1312		
5	2.98	≥80MHz	1050	1400	1381	1378	hot load in furnace
					1374		
6	2.98	≥80MHz	1050	1400	1304	1305	hot load in furnace
					1305		

is the centre of the band for which the VSWR is less than 1.2. The true temperature of the cathodes is obtained by applying a correction of $80°K$ (section 5.4.1). In the last column of table 6.1 the standard noise source that has been used is mentioned.

6.4 Discussion of the results

6.4.1 Comparison of experiments with theory

If the applied d.c. voltage V is zero, the measured noise temperature
should be equal to the temperature of the cathodes. For tubes No. 1 and
No. 2 (Figs. 6.5 and 6.6) we find a noise temperature that is some 70°
below cathode temperature. This discrepancy should for the greater part
be attributed to the absorption of the noise signal by a thin metal layer
on the glass wall. As already mentioned in section 5.4.2, this layer is
caused by evaporation of metal (presumably Ba) from the cathodes during
the life of the tube.

In order to verify this, we measured, with V = 0, the noise tempera-
tures of tubes No. 3 and No. 5, which had not been used in measurements
before. For both tubes the first measurements gave a noise temperature
that was 20° below cathode temperature (table 6.1). Also, tube No. 3
showed a decreasing noise temperature when being subjected to a long se-
ries of measurements.

The remaining discrepancy of 20° found in a new tube can partly be at-
tributed to the inaccuracy of the determination of the cathode tempera-
ture and partly to the systematic errors in the attenuation factors a and
b (see Eqs.(6.1) and (6.2)). The accuracy with which the black body tem-
perature can be determined by means of a pyrometer is about 10°. The ac-
curacy of the correction that has to be applied in order to obtain the
true temperature, can also be estimated to be 10°. The possible errors in
a and b are of the order of magnitude of 0.05 dB, i.e. 15°. The deviation
found for tubes No. 3 and No. 5 can thus be well accounted for.

If we apply a voltage across the double-cathode tube, we find both
theoretically and experimentally that the noise temperature decreases.

However, experimentally a smaller decrease is found than the calculated values would suggest. We have no explanation for this difference.

6.4.2 The double-cathode tube as a thermal noise source

As already discussed in chapter 1, if no voltage is applied to a double-cathode tube, its noise can be considered either as thermal noise or as shot noise. When considering its noise temperature if $V \neq 0$, we are, in fact, studying how much it differs from a thermal noise source. Instead of comparing its noise temperature with the temperature of the cathodes, we may also compare it with a temperature defined by means of the random kinetic energy $<W_r>$ per electron, i.e. the average kinetic energy $<W>$ per electron minus the average drift-energy per electron.

To that end we first calculate the average kinetic energy $<W>$ per electron for the whole inter-electrode space. Let $Q(x)dx$ be the sum of the kinetic energies of the electrons in a layer with an area of 1 m^2 and a thickness dx situated at x:

$$Q(x) = \tfrac{1}{2} m \int v^2 \, n(x,v) \, dv \tag{6.3}$$

The integration has to be performed over all velocities that occur at x. Using Eqs.(2.3), (2.5) and (2.6), it is found that

$$Q(x) = B\left[\left(\frac{d\eta}{d\xi}\right)^2 + 1 + \exp(\eta_{c1} - \eta_{c2})\right] \tag{6.4}$$

where

$$B = (2\pi kTm)^{\tfrac{1}{2}} \frac{1}{4q} J_s \exp(-\eta_{c1})$$

The total number of electrons is given by the following expression:

102

$$N_t = \int_0^d n(x) \, dx \qquad (6.5)$$

Integrating Eq.(6.4) with respect to x, and using Eqs.(6.5) and (2.10), yields $\langle W \rangle = 1.12 \times 10^{-20}$ joule, if the applied voltage = 0.5 volt, the distance d = 55 microns, the temperature of the cathodes (area = 1 m^2) = = 1300°K, and the saturation current density = 3.54 A/cm^2. The average kinetic energy $\langle W \rangle$ is about 20% higher than $\frac{1}{2}$kT.

Secondly, we calculate the average drift-energy per electron. Let w(x) be the drift velocity at x. It is given by the following expression:

$$w(x) = \int v \, n(x,v) \, dv \bigg/ \int n(x,v) \, dv$$

where the integration has again to be performed over all possible velocities. The drift energy per electron between x and x+dx is $\frac{1}{2}$mw^2(x). From this it is easy to find the average drift-energy per electron in the whole inter-electrode space:

$$\frac{1}{2} \frac{m}{N_t} \int_0^d n(x) \, w^2(x) \, dx = c \int_0^d \frac{dx}{n(x)} \qquad (6.6)$$

with

$$c = \frac{1}{2} \frac{m}{q^2 N_t} J_s^2 \left\{ \exp(-\eta_{c1}) - \exp(-\eta_{c2}) \right\}^2$$

Subtracting the average drift-energy, expressed by Eq.(6.6), from $\langle W \rangle$, yields a value for the random kinetic energy $\langle W_r \rangle$ per electron that is some 5% higher than $\frac{1}{2}$kT, if V = 0.5 volt. In Fig. 6.7 the average kinetic energy $\langle W \rangle$ and the random kinetic energy $\langle W_r \rangle$ per electron are also plotted for other values of the voltage V. It seems that the tube is not far

103

from thermal equilibrium. Still, the noise temperature does not increase when raising the voltage, as suggested by the above results, but decreases.
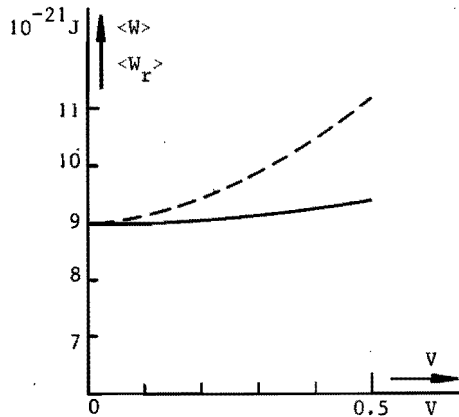

Fig. 6.7. Average kinetic energy <W> per electron (dotted line) and random kinetic energy <W_r> per electron (solid line) vs. the applied d.c. voltage V. Temperature of cathodes = 1300°K, saturation current density = = 3.54 A/cm^2; distance d = 55 μm.

Finally, we mention the surprising result obtained from numerical calculations that the total number N_t of electrons is practically independent of the d.c. voltage V for the range considered in Fig. 6.7.

6.4.3 The double-cathode tube as a source of shot noise

While we considered in the previous section the deviations of the noise of the tube from that expected by treating it as thermal noise, we shall now study the deviations from shot noise, as given by Eq.(1.4).

Let us determine the noise suppression factor Γ^2 as defined in chapter 1. As stated there, Γ^2 is equal to unity al low frequencies if V = 0. At 3

GHz, however, we find $\Gamma^2 = 0.459$ for $V = 0$, using the equality

$$4 \ k \ T_n \ \text{ReY} \ \Delta f = 4 \ q \ I \ \Gamma^2 \ \Delta f \tag{6.7}$$

which was derived from Eqs.(1.1) and (1.6). Since the noise is not sup-pressed by the potential minimum in this case, the noise suppression is obviously caused by transit-time effects.

On the other hand, if the voltage between the cathodes is high, the double-cathode tube behaves as a normal diode. At low frequencies the noise suppression factor of a normal diode is (Cf. reference[6],p.96):

$$\Gamma^2 = \frac{9}{4} \ (4-\pi) \ \frac{1}{\eta_{c2}} \tag{6.8}$$

If we apply this formula to our tube at $V = 0.5$ volt, we find $\Gamma^2 = 0.250$. At 3 GHz we can calculate Γ^2 under similar conditions with the help of the
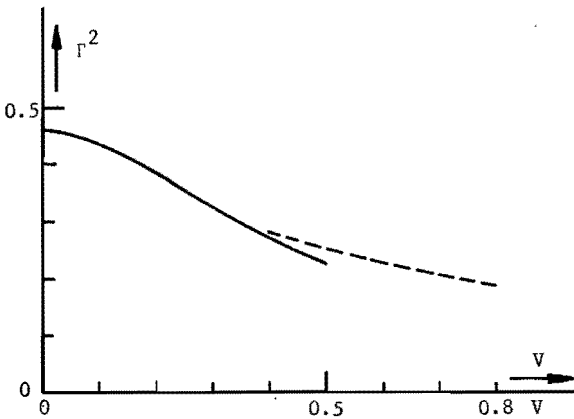

Fig. 6.8. Noise suppression factor Γ^2 vs. d.c. voltage V at 3 GHz. The dotted line indicates the values of Γ^2 for a normal diode at low frequen-cies. See caption of Fig. 6.7 for other parameter values.

following expression

$$\Gamma^2 = \frac{2 k T_n \, ReY}{q(I_1 + I_2)} \qquad (6.9)$$

which is the same as Eq.(6.7), except that the sum of the two electron
currents $2I$ has been replaced by $I_1 + I_2$, the two currents not being the
same if $V \neq 0$. At $V = 0.5$ volt, Γ^2 is 0.229. These and other results ob-
tained with the aid of Eqs.(6.8) and (6.9) are shown in Fig. 6.8. The val-
ues of η_{c2} at $V = 0.6$, 0.7 and 0.8 volt, which have been substituted in
Eq.(6.8), were found by extrapolation of those known for $V = 0(0.1)0.5$
volt. It turns out that for voltages of over 0.4 volt the values of Γ^2 for
the double-cathode tube at high frequencies are somewhat lower than the
corresponding ones for the normal diode at low frequencies. This is due to
transit-time effects.

REFERENCES

1. North, D.O., R.C.A. Review 4 (1939/40) 441-472.

2. Lindsay, P.A. and F.W. Parker, J. Electr. Control 7 (1959) 289-315.

3. Knol, K.S. and G. Diemer, Philips Res. Repts. 5 (1950) 131-152.

4. Lindsay, P.A., contribution to:

   Marton, L.(Ed.) Advances in electronics and electron physics, XIII,

   Academic Press, New York (1960) 181-315.

5. Von Laue, M., Jahrbuch Radioaktivität Elektr. 15 (1918) 205-256.

6. Van der Ziel, A., Noise, Prentice-Hall, Englewood Cliffs, N.J. (1956).

7. Paucksch, H., Nachrichtentechn. Z. 9 (1956) 410-414.

8. Löcherer, K.-H., Archiv E.Ü. 12 (1958) 225-236, 265-270.

9. Hubert, H., Proc. MOGA 68, Nachrichtentechnische Fachberichte 35,

   327-332, V.D.E. Verlag, Berlin, 1968. See also: Hubert, H., Disserta-

   tion, Technische Universität Berlin (1969).

10. Thompson, B.J., R.C.A. Review 4 (1939/40) 269-285.

11. Whittaker, E.T. and G.N. Watson, A course of modern analysis, Univer-

    sity Press, Cambridge (1963).

12. Taylor, A.E., Introduction to functional analysis, John Wiley, New

    York (1958) pp. 277 and 284.

13. Llewellyn, F.B. and A.E. Bowen, Bell Syst. T.J. 18 (1939) 280-291.

14. Fox, L. (Ed.), Numerical solution of ordinary and partial differential

    equations, Pergamon, Oxford (1962), Chapter 11.

15. Zonneveld, J.A., Automatic numerical integration, Mathematisch Cen-

    trum, Amsterdam (1964).

16. Paucksch, H., Archiv E.Ü. 9 (1955) 171-176.

17. Isaacson, E. and H.B. Keller, Analysis of numerical methods, John

    Wiley, New York (1966), Section 6.2 of chapter 7.

18. Van der Meijden, P.J.H., Internal report EEA/53/1969, Dept. of Electrical Engineering, Eindhoven University of Technology.

19. Versnel, W., Proc. MOGA 70, Eighth int. conf. on microwaves and optical generation and amplification, pp. 18/19-18/23, Kluwer, Deventer (The Netherlands), 1970.

20. Hennings, K., Nachrichtentechn. Z., 12 (1959) 459-464.

21. Kato, N. and T. Isobe, Mem. Fac. Eng. Kyoto Univ. 20 (1958) 27-47 (Part I) and 20 (1958) 48-71 (Part II).

22. Dye, N.E., J. Hessler, A.J. Knight, R.A. Miesch and G. Papp, 1959 IRE National Convention Record 7, part 3, 40-46.

23. Bronwell, A.B., T.C. Wang, I.C. Nitz, J. May and H. Wachowski, Proc.

24. Van Iperen, B.B. and H. Tjassens, Proc. MOGA 70, Eighth int. conf. on microwaves and optical generation and amplification, pp. 7/27-7/32, Kluwer, Deventer (The Netherlands), 1970.

25. Groendijk, H. and W. Versnel, Appl. Sci. Res. 21 (1969) 309-321.

26. Heijnemans, W.A.L., Internal report ETA/4/1970, Dept. of Electrical Engineering, Eindhoven University of Technology.

27. Deschamps, G.A., J. Appl. Phys. 24 (1953) 1046-1050.

28. Storer, J.E., L.S. Sheingold, S. Stein, Proc. IRE 41 (1953) 1004-1013.

29. Pieterse, J.D. and W. Versnel, Appl. Sci. Res. 21 (1969) 13-23.

30. Lewin, L., Wireless Engineer 26 (1949) 258-264.

31. Kajfez, D., IEEE Trans. MTT-18 (1970) 96-100.

32. Espe, W., Werkstoffkunde der Hochvakuumtechnik I, Deutscher Verlag der Wissenschaften, Berlin (1960), p. 896.

33. Wells, J.S., W.C. Daywitt and C.K.S. Miller, IEEE Trans. IM-13 (1964) 17-28. Further, see the "Special issue on noise" of IEEE Trans. MTT-16 (1968) No. 9.

34. Groendijk, H., Philips T.T. 19 (1957) 383-385.

35. Hart, P.A.H., Philips T.T. 23 (1961) 284-301.

Acknowledgements

Samenvatting

Wanneer men bij een vlakke diode de anode eveneens als kathode uit-
voert, ontstaat er een dubbel-kathodebuis. De bestudering van de eigen-
schappen van een dergelijke buis bij hoge frequencies, wanneer deze in
het ruimteladingsgebied is ingesteld, vormt het onderwerp van dit proef-
schrift. Hoogfrequent betekent in dit verband, dat de looptijden van de
elektronen niet verwaarloosd mogen worden.

De bewegingen van de elektronen in een dubbel-kathodebuis kunnen on-
derzocht worden op dezelfde manier als in de theorie van de gewone diode
gebeurt. Dit geldt zowel voor lage frequenties, waarbij de looptijden ver-
waarloosd worden, als voor hoge frequenties. In het eerste geval levert
de theorie o.a. de stationaire potentiaalverdeling, waarbij evenals bij
een normale diode een potentiaalminimum gevonden wordt.

In het bizondere geval, dat de kathoden dezelfde temperatuur en de-
zelfde potentiaal bezitten, ligt dit minimum midden tussen beide kathoden.
De potentiaalverdeling is dan nl. symmetrisch. Dit geval is daarom zo in-
teressant, omdat dan de elektronenwolk in thermodynamisch evenwicht is met
de kathoden. Een gevolg hiervan is, dat de ruis die de buis kan afgeven,
hetzij als thermische ruis hetzij als shotruis beschreven kan worden.
Een overzicht van de eigenschappen van een dubbel-kathodebuis bij lage
frequenties is in hoofdstuk 2 gegeven.

Bij hoge frequenties kunnen, zoals reeds vermeld is, de looptijden
van de elektronen niet meer verwaarloosd worden. Het is mogelijk in dat
geval het gedrag van de buis te beschrijven met behulp van twee integraal-
vergelijkingen in de hoogfrequente elektrische veldsterkte. Met behulp
van deze veldsterkte kunnen de admittantie en de ruis van de dubbel-ka-
thodebuis berekend worden. In hoofdstuk 3 is de theorie behandeld, ter-
wijl in hoofdstuk 4 de numerieke uitwerking is weergegeven. Eén van de
resultaten van de theorie is, dat zowel het reële als het imaginaire deel

van de hoogfrequente elektronische admittantie, d.w.z. de admittantie die een gevolg is van de elektronen alleen, met toenemende gelijkspanning tussen de kathoden groter wordt. Dit is juist andersom als bij lage frequenties waar de (hier uiteraard reële) elektronische admittantie juist afneemt bij toenemende gelijkspanning. Dit is een gevolg van de relatief grote looptijden bij hoge frequenties. Bij zeer korte afstanden (20 μm), waar de looptijden kleiner zijn vinden wij dan ook bij hoge frequenties hetzelfde verloop als bij lage frequenties. Een ander resultaat is, dat de ruistemperatuur van de buis afneemt bij toeneming van de aangelegde gelijkspanning (tot 0.5 volt).

In hoofdstuk 5 wordt vervolgens onderzocht, wat het effect is wanneer een dergelijke buis opgenomen wordt in een golfpijpcircuit. Het blijkt, dat bij juiste keuze van de referentievlakken, ten opzichte waarvan het equivalente microgolfnetwerk van de buis bepaald is, de dubbel-kathode-buis door één enkele relatieve impedantie goed beschreven kan worden. Theoretische en experimentele resultaten worden, voor wat betreft de elektronische admittantie van de buis, met elkaar vergeleken. Gezien de complexe structuur van het theoretische model is er een redelijke overeenstemming van theorie en praktijk.

De berekeningen stellen ons in staat een inzicht te krijgen in de processen, die in het inwendige van de buis plaats vinden bij het aanleggen van een kleine hoogfrequente wisselspanning tussen de kathoden. Het blijkt, dat de verschijnselen beschreven kunnen worden door middel van twee uitdovende ruimteladingsgolven, die met nagenoeg tegengestelde fasen vanaf de kathoden naar binnen lopen. Op hun ontmoetingspunt hebben zij een amplitude nul en verschillen zij 180° in fase. Dit punt, waar de ruimtelading dus constant is, valt waarschijnlijk samen met het minimum van de ruimteladingsdichtheid.

Tenslotte worden in het laatste hoofdstuk de ruismetingen behandeld. Het blijkt bij deze metingen noodzakelijk te zijn, dat de buis is opgenomen in een golfpijp met een kleinere hoogte dan die van de standaardgolfpijp. In dat geval kan aanpassing over een voldoend breed frequentiegebied van de buis aan de golfpijp gerealiseerd worden. Ook hier wordt een redelijke overeenstemming tussen theorie en experiment gevonden.

Als de kathoden op dezelfde spanning staan zijn de voor de ruis gevonden waarden kleiner dan de met de formule voor de shotruis berekende waarden. Er kan daarom een ruisonderdrukkingsfactor Γ^2 bepaald worden. Deze wordt vergeleken met de waarde $\Gamma^2 = 1$, welke voor lage frequenties geldt.

Bij relatief hoge gelijkspanningen gedraagt de buis zich als een normale diode. Ook hier blijkt Γ^2 bij hoge frequenties kleiner te zijn dan bij lage frequenties. De afwijkingen zijn een gevolg van looptijdeffecten.

Curriculum vitae.

20 juni 1933 : Geboren te Rotterdam.

 8 juli 1950 : H.B.S.-B examen te Rotterdam (Libanon-H.B.S.)

28 febr.1956 : Examen van Natuurkundig Ingenieur aan de Technische

                Hogeschool te Delft. Afgestudeerd bij Prof.Dr. H.B. Dor-

                gelo op een spectroscopisch onderwerp.

   1956-1957 : Militaire dienst.

 3 dec. 1958 : Kandidaatsexamen Wis- en Natuurkunde A aan de Universi-

                teit van Amsterdam.

 1 jan. 1959 : Wetenschappelijk medewerker bij het Mathematisch Centrum

                te Amsterdam.

 1 april 1960 : Wetenschappelijk medewerker bij de Afdeling der Elektro-

                techniek aan de Technische Hogeschool te Eindhoven.

STELLINGEN

I

Door Lindsay's theorie betreffende de potentiaalverdeling in een dubbel-
kathodebuis welke in het ruimteladingsgebied is ingesteld, te combineren
met de ruistheorie van North voor de gewone diode kan een generalisatie
van de laatste theorie verkregen worden. Deze gegeneraliseerde theorie be-
schrijft de ruis van een dubbel-kathodebuis bij lage frequenties.

> 1) *Lindsay, P.A., bijdrage tot: Marton, L.(Ed.),*
>
> *Advances in electronics and electron physics, XIII,*
>
> *Academic Press, New York, 1960, blz. 243.*
>
> 2) *North, D.O., R.C.A. Review 4 (1939/40) 441-472.*

2

De ruistheorie bij lage frequenties, vermeld in bovenstaande stelling, is
niet af te leiden uit de in dit proefschrift gegeven ruistheorie door
daarin de frequentie tot nul te laten naderen.

> *Dit proefschrift, § 3.7.*

3

Het is mogelijk een Onsager-relatie op te stellen voor de dubbel-kathode-
buis.

> *De Groot, S.R., Thermodynamics of irreversible processes,*
>
> *North-Holland Publ. Cy, Amsterdam, 1966.*

4

Bij microgolfmetingen aan een inductief obstakel in een golfpijp, bestaan-
de uit twee cirkelcylindrische paaltjes met een spleet er tussen, waarvan
de breedte instelbaar is, treedt in het algemeen een sprong in de reflec-
tie op bij de overgang van positieve spleetbreedte naar spleetbreedte = 0.
In dat geval staan de twee eindvlakken van de paaltjes niet geheel even-
wijdig ten opzichte van elkaar.

Groendijk, H. and W. Versnel, Appl. Sci. Res. 21 (1969)
309-321.

5

De ruistemperatuur van de K51A, een gasontladingsbuis, is ongeveer
17.000^{o}K in plaats van 23.600^{o}K, waarop Wittig zijn ruismetingen aan een
vacuumdiode bij 2,4 GHz baseert. Ook de ruismetingen bij 3 GHz van
Prinzler aan de K51A zijn onjuist.

1) Wittig, G., Nachrichtentechn. Z. 16 (1963) 8-13.
2) Prinzler, H., Proc. second coll. on microwave communication,
Akadémiai Kiadó, Budapest, 1963, blz. 261-273.

6

Bij frequentie-stabilisatie van een 4mm-klystron met behulp van de
"phase-locking" techniek, waarbij als referentie een kwartskristal ge-
bruikt wordt, kan volstaan worden met slechts één "phase-locked loop" in
plaats van twee.

1) Meier, G., Z. Angew. Physik 16 (1964) 466-471.
2) French, I.P. and T.E. Arnold, Rev. of Sci. Instr. 38
(1967) 1604-1607.

7

Het is mogelijk een gesloten trilholte voor 8mm-golven te maken, welke,
op kamertemperatuur gehouden, bij kritische aankoppeling een "loaded" kwa-
liteitsfactor groter dan 10.000 bezit.

Otto, W., Nachrichtentechnik 10 (1960) 365-372.

8

Vraagstukkenboeken dienen enkele uitgewerkte voorbeelden en alle ant-
woorden te bevatten. Uitwerking van alle vraagstukken is vanuit didactisch
standpunt gezien onjuist.

9

"Multiple choice" examens zijn zeer geschikt om feitenkennis te testen.
Des te exacter een vak is, des te minder leent zich deze methode om een
oordeel te verkrijgen over het inzicht van de examinandus.

10

Een digitale rekenmachine, welke op meesterniveau zou kunnen schaken, kan
in verband met practische overwegingen niet gerealiseerd worden.

Botvinnik, M.M.; Computers, chess and longe-range planning,
Springer, New York, 1970.

W. Versnel,   Eindhoven, 14 mei 1971